

https://dspace.org/

# Debunking the impact of crystalliteparticle size in cobaltbased fischertropsch synthesis

**J GORIMBO; Roick Chikati; P Khangale; I.N Beas; L.L Mguni ...**

TAYLOR & FRANCIS INC
https://hdl.handle.net/10539/43417
WOS

Downloaded from a DSpace repository. https://dspace.org/



Chemical Engineering Communications

ISSN: (Print) (Online) Journal homepage: www.tandfonline.com/journals/gcec20

# Debunking the impact of crystallite/particle size in cobalt-based Fischer-Tropsch synthesis

Joshua Gorimbo, Roick Chikati, Phathutshedzo Khangale, Isaac N. Beas, Liberty L. Mguni & Diankanua Nkazi

**To cite this article:** Joshua Gorimbo, Roick Chikati, Phathutshedzo Khangale, Isaac N. Beas, Liberty L. Mguni & Diankanua Nkazi (2024) Debunking the impact of crystallite/particle size in cobalt-based Fischer-Tropsch synthesis, Chemical Engineering Communications, 211:8, 1262-1287, DOI: 10.1080/00986445.2024.2341263

**To link to this article:** https://doi.org/10.1080/00986445.2024.2341263

© 2024 The Author(s). Published with license by Taylor & Francis Group, LLC

Published online: 06 May 2024.

Submit your article to this journal

Article views: 730

View related articles

View Crossmark data

Full Terms & Conditions of access and use can be found at https://www.tandfonline.com/action/journalInformation?journalCode=gcec20

CHEMICAL ENGINEERING COMMUNICATIONS
2024, VOL. 211, NO. 8, 1262–1287
https://doi.org/10.1080/00986445.2024.2341263

Taylor & Francis
Taylor & Francis Group

REVIEW ARTICLE

OPEN ACCESS Check for updates

# Debunking the impact of crystallite/particle size in cobalt-based Fischer-Tropsch synthesis

Joshua Gorimbo[a], Roick Chikati[b], Phathutshedzo Khangale[a], Isaac N. Beas[c], Liberty L. Mguni[a], and Diankanua Nkazi[b]

[a]Institute for the Development of Energy for African Sustainability (IDEAS), College of Science, Engineering and Technology, University of South Africa (UNISA), Johannesburg, South Africa[b]Department of Chemical and Metallurgical Engineering, University of the Witwatersrand, Johannesburg, South Africa; [c]Department of Natural Resources & materials, Botswana Institute for Technology Research and Innovation Gaborone, Botswana, South Africa

**ABSTRACT**

This review examines the relationship between the crystallite size of cobalt and the distribution of products produced by Fischer-Tropsch synthesis (FTS). The ideal range for the average cobalt crystallite diameter is between 6 and 8 nm. Deviating from this range, whether by increasing or decreasing the crystallite size, influences the carbon monoxide (CO) turnover frequency and the selectivity of $CH_4$, $C_2$-$C_4$, and $C_{5+}$. To ensure the development of a consistent catalyst, careful monitoring and adjustment of the morphology, particle size, and metal loading on the support particles are essential. For experimental repeatability during FTS applications, it would be ideal if catalyst particles had crystallites of a uniform size. Methods for crystallite characterization and catalyst synthesis were also addressed in detail. The diameter of the cobalt crystallite appears to be a crucial parameter that influences cobalt oxidation, the thermodynamics of cobalt reduction and oxidation are reported. Conducting a Design of Experiment (DOE) with Design Experts on available literature led to determining optimal conditions for enhancing the primary target product of FTS—$C_{5+}$ selectivity.

**KEYWORDS**

$C_{5+}$ selectivity; cobalt oxidation; cobalt reduction; crystallite size Fischer-Tropsch synthesis (FTS); design of experiments

## Introduction

Fischer-Tropsch Synthesis (FTS) is a catalytic process transforming syngas (carbon monoxide and hydrogen) into valuable hydrocarbons (Deugd et al. 2001). Transition metals like cobalt, iron, or ruthenium serve as catalysts in this reaction. With a growing emphasis on sustainable energy solutions globally, FTS plays a significant role in generating clean and renewable hydrocarbons, helping reduce reliance on conventional fossil fuels and addressing environmental concerns (Hu et al. 2012). The Fischer-Tropsch reaction scheme involves a series of reaction steps where syngas react over a suitable catalyst to yield hydrocarbons. The generalized reaction can be represented as shown in Equation (1). There has been a proliferation of studies on the effect of the size of cobalt crystallite in FTS catalytic systems when tailoring product distribution by controlling both particle and crystallite size (Bezemer et al. 2006; Herranz et al. 2009; Rane et al. 2012; Fischer et al. 2014; Fu et al. 2014; Yang et al. 2016; Fang et al. 2020). Different synthesis methods have been employed to yield the required cobalt crystallite size or a specific cobalt diameter on the surface of different supports. For instance, various 10%Co/ITQ-2 zeolites model catalysts were synthesized by combining reverse micellar and surface-silylated ITQ-2 delaminated zeolite to yield a $Co^0$ crystallite size distribution in the 5–11 nm range (Prieto et al. 2009). In another study, cobalt crystallite ranging from 2.6 to 16 nm was prepared, using incipient wetness impregnation, by controlling the cobalt loading from 1 to 22 wt% and varying the cobalt precursor used ($Co(NO_3)_2xH_2O$ or $Co(CH_3CO_2)_2 \cdot 4\,H_2O$) or the solvent used ($H_2O$ or EtOH)

CONTACT Liberty L. Mguni leemguni@gmail.com; Joshua Gorimbo joshuagorimbo@gmail.com Institute for the Development of Energy for African Sustainability (IDEAS), College of Science, Engineering and Technology, University of South Africa (UNISA), Johannesburg, South Africa.

© 2024 The Author(s). Published with license by Taylor & Francis Group, LLC
This is an Open Access article distributed under the terms of the Creative Commons Attribution-NonCommercial-NoDerivatives License (http://creativecommons.org/licenses/by-nc-nd/4.0/), which permits non-commercial re-use, distribution, and reproduction in any medium, provided the original work is properly cited, and is not altered, transformed, or built upon in any way. The terms on which this article has been published allow the posting of the Accepted Manuscript in a repository by the author(s) or with their consent.

(J. Den Breejen et al. 2009). Borg et al. (2008) prepared cobalt catalysts with crystallite sizes of 3 to 18 nm using one-step incipient wetness impregnation of alumina supports ($\gamma$ and $\alpha$-$Al_2O_3$), with a variety of cobalt nitrate solutions-such as water, ethylene glycol, diethylene glycol, or their combinations. The general observation in all these experiments is the intricacies of preparing a catalyst with crystallites of a certain size.

$$2nH_2 + nCO \rightarrow -C_nH_{2n} - +nH_2O \quad (1)$$

where $n$ represents the number of carbon atoms in the hydrocarbon product.

The literature shows that different crystallite sizes of the supported cobalt catalyst behave differently during reduction and the Fischer-Tropsch (FT) reaction. Smaller cobalt crystallites (less than 6 nm) are more difficult to reduce than larger crystallites (20–70 nm) (Jacobs et al. 2007a). During the FT reaction, cobalt crystallites with a spherical shape and diameter less than 4.4 nm oxidize easily when $P_{H2O}/P_{H2} < 1.5$, according to van Steen et al. (2005). This suggests that controlling the size of the crystallite is important. The pore size of the support governs the diameter of the $Co_3O_4$ cobalt crystallite, with small crystallites forming in narrow support pores and large crystallites forming in wide pores (Borg et al. 2007).

The effect of support particle size is equally essential in FTS, as it affects reactant conversion selectivity. The smaller the support particle size, the larger the specific surface area of the support. Soykal et al. (2012) conducted experiments to evaluate the effect of the support particle sizes of Co/$CeO_2$ catalysts in ethanol steam reforming. When comparing two support particles of different sizes (μm range and nm range), they observed that particles in the nm range show better ethanol reforming activity and deliver a higher ethylene yield. The benefit of being highly resistant to coking was observed with catalysts supported on particles in the nm range, whereas larger ceria particles in the μm range were prone to coke formation.

Researchers use a wide range of support particle sizes in FTS systems. For instance, in a study by Tsubaki et al. (2001), they employed silica gel particles ranging from 74 to ±590 μm, with support particles smaller than 149 μm. Den Breejen et al. (2009) utilized carbon nanofibers with a fraction size of 90–150 μm. Fu et al. (2014) opted for carbon nanotubes (CNT) with a particle size of 180 − 425 μm. Saib et al. (2002) used silica with a particle size ranging from 212 to 250 μm. Rane et al. (2012) used utilized alumina with a size range of 53–90 μm mixed with silicon carbide particles sized 75–150 μm. Because of these variations in particle size, further studies are needed to determine the statistical significance of such wide variations in support size. This analysis will face the challenge of metal-support interaction with different supports, each support having distinct surface properties, acidity levels, and metal-support interactions. Moreover, we also recognize the multifaceted interplay between cobalt particle size and support size. The correlation between these two parameters adds another layer of complexity to the analysis. Table 1 gives examples that demonstrate the effect of cobalt crystallite size on FTS reaction.

The choice of support size in FTS systems at industrial scale is a crucial aspect that is also dependent on the type of reaction system employed, whether it's a fixed-bed, Continuous Stirred-Tank Reactor (CSTR), or microchannel system, plays a pivotal role in determining the optimal support particle size. In fixed-bed systems, larger support particles might be preferred to minimize pressure drop but these large pellet diameters lead to greater diffusion limitations. Brunner et al. (2015b) also showed that the catalyst shape affected the amount of catalyst required to achieve a specified conversion. The typical pellet size range is 1 to 4 mm (Pratt 2012; Brunner et al. 2015b; Stamenić et al. 2018). On the other hand, in CSTRs or microchannel systems, where heat and mass transfer limitations can be more pronounced, using smaller support particles can be advantageous. The smaller particles facilitate improved heat and mass transfer, ensuring efficient contact between the reactants and the catalyst surface (Ratchananusorn 2007).

The particle size of catalysts remains a crucial factor in catalysis, even when these particles are aggregated into pellets. Various effects arise from the particle sizes that make up the pellets in catalysis, influencing key aspects of catalyst performance. The surface area of catalysts is significantly impacted by particle size, with smaller

**Table 1.** Effect of cobalt crystallite size on different supports in FTS.

| Support type | Reaction conditions, pressure, temperature, SV | Cobalt (Co) crystallite size | Characterisation method used to measure crystallite size | Effects in FTS | References |
|---|---|---|---|---|---|
| Silica | 239.83 °C, $H_2/CO = 2$). 1 bar | 1.4–10.5 nm | TEM | The water vapour easily oxidises Smaller Co particles (1.4–2.5 nm) during FTS. A 1.4-2.5 nm particle size results in lower TOF and higher selectivity to $CH_4$ Larger Co particles in the 3.5–10.5 nm range show no oxidation during FTS. A 3.5-10.5 particle size does not affect TOF and $CH_4$ selectivity. | (Z. J. Wang et al. 2012) |
| Silica | 250 °C, $H_2/CO = 2:1$) 5 bar | 3-11nm | TEM | The maximum activity displayed for Co particles of 10–11 nm in size. $CO_2$ hydrogenation increases with an increase in Co crystallite size from 3 to 11nm. C5+ maximum extent at 11 nm. | (Melaet et al. 2014) |
| Alumina | 210°C, $H_2/CO = 2.1$ 20 bar PS = 53–90 $\mu$m | 2–14 nm | XRD, $H_2$-chemisorption | When Co particle size increases, C5+ selectivity is maximised at a crystallite size of 8–9 nm. With larger particles, selectivity to $C_{5+}$ decreases before approaching a constant value. | (Rane et al. 2012b) |
| Alumina | 190 °C, $H_2/CO = 2$, 9.9 bar PS =150–200 $\mu$m | 2.3-11.7 nm | XRD, TEM | The selectivity of $CH_4$ varies inversely with a decrease in crystallite size and $C_{5+}$ selectivity. | (Fischer et al. 2013) |
| Alumina | 210°C, 20 bar, and $H_2/CO = 2.1$ PS = 53 and 90 $\mu$m | 3 to 18 nm | XRD, TEM, XPS | 7–8 nm Co particles yielded maximum $C_{5+}$ selectivity. $C_{5+}$ selectivity is constant for a crystallite size larger than 9–10 nm. | (Borg et al. 2008b) |
| Silica delaminated ITQ-2 zeolite. | 220°C, $H_2/CO = 2$ 20 bar PS = 0.25–0.42 mm | 5.6–141 nm | XRD, $H_2$-chemisorption and (HR)TEM | The activation energies $Co_3O_4$ reduction to CoO and Co crystallite size dependent, for particles ranging from 5.6 to141 nm. | (Prieto et al. 2009c) |
| Carbon nanofibers | 210, 220 and 250°C, $H_2/CO = 2$).1 and 35 bar PS = 0.5-1.0 mm and 150-212 $\mu$m | 2.6-27 nm | (TEM), EXAFS, XPS and $H_2$ chemisorption | FTS is not influenced by Co crystallite size >6 nm at 1 bar and >8 nm at 35 bar. Both TOF and $C_{5+}$ selectivity decreased when the crystallite size was decreased from 16 to 2.6 nm. | (G. Leendert Bezemer et al. 2006) |
| Carbon nanofiber | 220 °C, $H_2/CO = 2$).1 and 35 bar PS = 90-150 $\mu$m | 2.6-16 nm | TEM, $H_2$-chemisorption | Co particles <6 nm result in decreased TOF and increased CH4 selectivity. | (J. P. Den Breejen et al. 2009) |
| Activated carbon and on CNTs | 230°C, $H_2/CO = 2$, 20 bar PS = 180 − 425 $\mu$m | 2.5 – 20.3 | XRD, TEM | Co crystallite up to 7 nm displayed higher TOF and $C_{5+}$ selectivity. No effect was observed for a Co crystallite size greater than 7 nm on TOF and $C_{5+}$ selectivity. | (Fu et al. 2014b) |

Information not given. PS = particle size.

particles generally providing a larger surface area per unit mass. This heightened surface area enhances catalytic activity by exposing more active sites for reactions to occur (García-Sánchez and Baldovino-Medrano, 2023). Even when assembled into pellets, the overall surface area is influenced by the arrangement and packing of particles within the pellet.

Particle size also affects diffusion rates within the catalyst pellet. Smaller particles may mitigate diffusion limitations, facilitating easier access of reactants to active sites. However, the packing arrangement in the pellet can alter diffusion pathways, influencing overall diffusion rates (Thiele, 1939; Mitchell et al. 2013). The catalytic activity is closely linked to the size of active sites on the catalyst surface. Smaller particles may expose a higher proportion of active sites, potentially leading to increased catalytic activity (Zhou et al. 2010; García-Sánchez and Baldovino-Medrano, 2023). The arrangement of particles within the pellet, however, can impact the accessibility of these active sites to reactants. In some instances, smaller particles may result in higher mass transfer limitations due to increased fluid flow resistance. The assembly of these particles into pellets affects the porosity and permeability of the catalyst bed, influencing mass transfer limitations (Satterfield et al. 1969; Yang et al. 2010). The size of catalyst particles can influence the selectivity of catalytic reactions. Different particle sizes expose varying crystal facets or surface structures, impacting the selectivity for specific reaction pathways (Wang and Lu 2020).

The particle sizes constituting catalyst pellets in catalysis have multifaceted effects on overall catalyst performance. Achieving the desired catalytic performance involves a delicate balance between maximizing active surface area, ensuring efficient mass transfer, and maintaining stability within the catalyst bed. The design and optimization of catalysts take into account these factors to meet specific catalytic requirements.

The morphology and metal loading on support particles are other critical parameters for designing and developing catalysts for the FTS. The FTS process converts synthesis gas into liquid fuels and chemicals. These parameters play a crucial role in determining the activity, selectivity, stability, and lifetime of the catalysts. They also significantly impact the product distribution and quality of the FTS outcomes. Therefore, the optimization of these parameters is essential for the successful implementation of the FTS process (Parker et al. 2019).

The morphology of the catalyst refers to the shape and structure of the metal particles and the support. The morphology can influence the surface area, the dispersion, the coordination number, the electronic structure, and the exposure of different facets of the metal particles, which in turn affect the adsorption, activation, and dissociation of the reactants, the chain growth and termination of the products, and the rate and extent of the secondary reactions, such as cracking, isomerization, hydrogenation, and water-gas shift (Modekwe et al. 2021). The metal loading on the support refers to the amount or the weight percentage of the metal on the support. The metal loading can influence the dispersion, the reducibility, the stability, and the lifetime of the catalyst. Generally, higher metal loading leads to higher dispersion and reducibility, but lower stability and lifetime. Lower metal loading leads to lower dispersion and reducibility, but higher stability and lifetime. Therefore, carefully monitoring and adjusting the morphology, particle size, and metal loading on support particles for consistent catalyst development is crucial for achieving the desired FTS outcomes, such as high yield and quality of liquid fuels, low yield of methane and carbon dioxide, and optimal catalyst performance and durability.

Finally, the thermodynamics of cobalt catalyst reduction in FTS holds significant importance for several reasons. Firstly, the reduction process is a crucial step in activating the cobalt catalyst, transforming it from oxidized states to metallic cobalt. This activated state is what is active in FTS. The specific thermodynamic conditions during reduction, including temperature and pressure, impact the efficiency of the catalyst activation. Understanding and optimizing these conditions are vital for achieving the desired catalytic activity which then directs a certain product selectivity and stability of the cobalt catalyst. Therefore, a detailed understanding of the thermodynamics of cobalt catalyst reduction is

instrumental in designing and improving catalytic systems for efficient and economically viable Fischer-Tropsch processes.

In summary, understanding the impact of morphology, catalyst loading, crystallite and particle size in cobalt-based Fisher-Tropsch synthesis is crucial for optimizing catalytic performance. It allows for the tailoring of catalysts to enhance specific reaction pathways, ultimately improving product selectivity. By investigating size-dependent phenomena, researchers can gain insight into the intricate interplay between surface area, active sites, and catalytic activity, paving the way for more efficient and sustainable processes. Ma and Dalai (2021) recently reported a review on the effect of structure and particle size with an emphasis on TOF for Co, Fe and Ru. The current work reviewed the effect of crystallite size on carbon monoxide (CO) turnover frequency and selectivity of $CH_4$, $C_2$-$C_4$ and C5+.

This research aims to understand the effect of cobalt crystallite size on performance and selectivity in the FTS process, which converts synthesis gas (CO and $H_2$) into liquid fuels and chemicals. The size of the cobalt crystallites is a significant factor affecting the catalyst's activity, stability, and selectivity, along with the rate and extent of secondary reactions such as cracking, isomerization, hydrogenation, and water-gas shift. By comprehending how the size of cobalt crystallites influences product distribution, the study offers insights for future catalyst design and the development of more efficient and selective catalysts for FTS. This, in turn, can improve the economic and environmental viability of the process. The work further looked at the thermodynamics of cobalt catalyst reduction and characterization techniques for determining crystallite size. Understanding the thermodynamics of cobalt catalyst reduction is crucial for optimizing catalyst activation, improving energy efficiency in FTS and contributing to the fundamental understanding of the process.

## Influence of cobalt particle size in FTS

Several catalyst preparation methods are used for FTS reactions. The different catalysts are made up of active components (usually transition metals), which are deposited on inert supports, such as titania, silica, alumina, and carbon. These supports improve certain properties, such as the stability of the active component and its dispersion. Precipitation and deposition impregnation are the main methods used to prepare the catalyst (Bianchi et al. 2001), though other methods exist, specifically for the FTS reaction (Bianchi et al. 2001; Tsubaki et al. 2001; Brunner et al. 2015a; Deraz 2018). The chosen synthesis method and cobalt loading affects catalyst morphology, i.e., crystallite size, pore size distribution, pore volume, surface area and promoter distribution (Deraz 2018), which eventually affects product distribution (Zhai et al. 2013; Ghogia et al. 2021). A review done by Deraz (2018) on the comparative jurisprudence of catalyst preparation methods focused on impregnation and precipitation methods and clarified the advantages and disadvantages of each technique. The goals of a study should define the selection of the catalyst preparation method. The impregnation method is often chosen because of its simplicity: the procedure is quicker and cheaper than some other methods and the catalyst properties and configuration can be tailored.

Figure 1 presents the effect of cobalt crystallite size on methane selectivity. The figure suggests that $CH_4$ selectivity is favorable for a cobalt crystallite size less than 6 nm and there is a negligible effect on larger crystallite sizes. The methane selectivity shown in Figure 1 differs in magnitude, but more importantly, the significant aspect is the pattern displayed and the flattening of the curve after approximately 8 nm. The tabulated literature results (Table 1) show that crystallite size affects catalyst activity and product selectivity. Larger cobalt particles (>7 nm) favor higher TOF and $C_{5+}$ selectivity. For cobalt crystallites ≥7 nm, $CH_4$ selectivity is suppressed (Fu et al. 2014). In a study carried out by Wang et al. (2012) using steady-state isotopic transient kinetic measurements, it was reported that reduced TOF for Co crystallite <6 nm is attributable to lower intrinsic activity at the small terraces and to the blocking of edge/corner sites (to a significant extent). The proclivity of small Co crystallite (<6 nm) to favor high production of $CH_4$ under FTS conditions is mainly due to higher coverage of the surface by hydrogen (Den Breejen et al. 2009). It should be

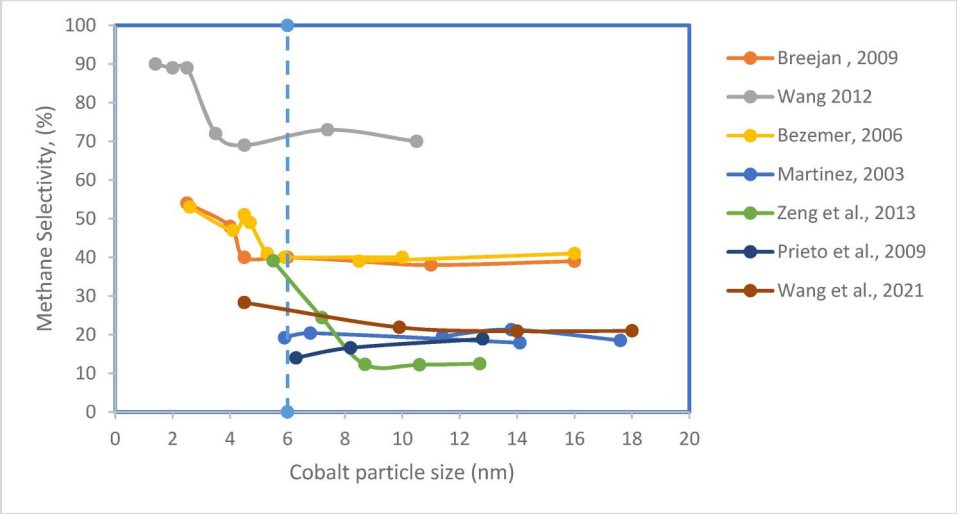



**Figure 1.** The increase in cobalt crystallite size on $CH_4$ selectivity: 220 °C, H2/CO = 2, 1 bar (Bezemer et al. 2006); 210 °C, $H_2$/CO = 2, 1 bar (Den Breejen et al. 2009); 220 °C, H2/CO = 2, 1 bar (Martínez et al. 2003); 239 °C, $H_2$/CO = 2, 1 bar $H_2$/CO = 2, P = 20 bar, 210 °C (Zeng et al. 2013); 220 °C, $H_2$/CO = 2, 20 bars (Prieto et al. 2009); 240 °C, $H_2$/CO = 2, P = 20 bar (Wang et al. 2021) [data used to generate this graph was obtained from the references given].

noted that turnover rates in FTS are not affected by Co crystallite dispersion and the type of support used over the accessible dispersion range under typical FTS conditions (Iglesia 1997a).

The activity of the FTS catalyst and its selectivity to desirable $C_{5+}$ hydrocarbons are important production design criteria to consider. Figure 2 shows the relationship between cobalt crystallite size and $C_{5+}$ selectivity. Borg et al. (2008) conducted a series of studies on Co supported on $\gamma$-$Al_2O_3$ and observed that $C_{5+}$ selectivity increases sharply with an increase in crystallite size up to about 7 nm (Figure 2), with the optimum crystallite size being about 8 nm. The figure also shows a negligible increase in selectivity for crystallites larger than 9–10 nm (Borg et al. 2008).

A correlation between $CH_4$ and $C_{5+}$ selectivity can be deduced from the available literature. Thus, a minimum $CH_4$ selectivity and maximum $C_{5+}$ selectivity are recorded with larger cobalt crystallites, while the opposite is true for smaller sizes. A similar pattern is observed during FTS in a packed bed: when indigenous water accumulates, $C_{5+}$ selectivity increases, whereas $CH_4$ selectivity decreases (Iglesia 1997a). A study done by Bezemer et al. (2006) supports the view that turnover frequency (TOF) and $CH_4$ selectivity remain unchanged for catalysts with a cobalt crystallite size greater than 6.0 nm, while a crystallite size of less than 6 nm results in variations in both

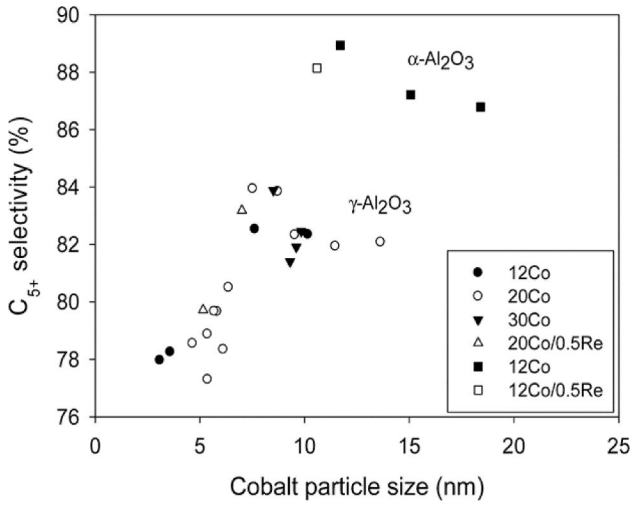



**Figure 2.** Depiction of the relationship between $C_{5+}$ selectivity and cobalt crystallite size. Source: Reproduced from (Borg et al. 2008) with permission from [Elsevier]. Copyright [2008].

selectivity and activity. It can, therefore be concluded that the ideal cobalt crystallite size should be greater than 6 nm. A study done by Bezemer et al. (2006) revealed that the TOF for hydrogenation of CO was not affected by a cobalt crystallite size greater than 6 nm at 1 bar and greater than 8 nm at 35 bar. Several researchers agree that TOF, a surface-specific activity, decreases with a decrease in cobalt crystallite size from about 1 to 7 nm (Den Breejen et al. 2009; Fu et al. 2014). Factors like the type of support used and metal dispersion have been reported to not have an effect on the turnover rate; hence, the activity of

the catalyst ought to be proportionate to the number of active sites (Martínez et al. 2003).

$Co_3O_4$ crystallite size is influenced significantly by the pore size of the support. A larger pore favors the formation of larger $Co_3O_4$ crystallites. A study by Song and Li (2006) indicated that catalysts with a 6–10 nm pore size produce a moderate $Co_3O_4$ crystallite diameter, consequently yielding the required selectivity. In a study done by Liu et al. (2007), increasing the pore size of the FTS catalyst from 2.9 to 12.6 nm had a positive impact: catalytic activity, $C_{5+}$, $C_{12}$–$C_{18}$, and $C_{18+}$ selectivity increased, and an antagonistic effect on $CH_4$ selectivity was observed. The higher $\alpha$ values obtained in a study by Rytter et al. (2018) were attributed to larger pore size and larger cobalt crystallites, which positively affect CO activation. Therefore, pore size is generally a selectivity director. The pore size of the support may control the size of the $Co_3O_4$ cobalt crystallite, as smaller crystallites form in narrow pores, whereas larger crystallites form in larger pores (Borg et al. 2007).

The data used to construct Figures 3 to 5 were extracted from various literature sources (Saib et al. 2002; Martínez et al. 2003; Song and Li 2006; Lira et al. 2008; Witoon et al. 2011). These sources provided the experimental conditions, catalyst type, catalyst analysis results and product distribution in terms of $C_1$, $C_2$-$C_4$, and $C_5$ selectivity. FT data for DOE was based on prior research on cobalt-impregnated silica support structures done by a group of academics, as reported in the available literature. Using the response surface approach, the effects of numerous independent and dependent variables were investigated. Design–Expert 13 was used to generate the 3-D plots. In terms of the data given, smaller cobalt crystallites of less than 12 nm proved to be more selective to methane. Increasing the crystallite size resulted in a decrease in methane selectivity. This observation concurs with the details provided in Table 1. Increasing pressure has a negligible effect on the conditions given.

$C_2$–$C_4$ selectivity decreases as crystallite size increases from 3 nm to about 15.8 nm, then gradually increases until it reaches 26 nm, see Figure 4. Smaller crystallites of 3 to 7.6 and larger

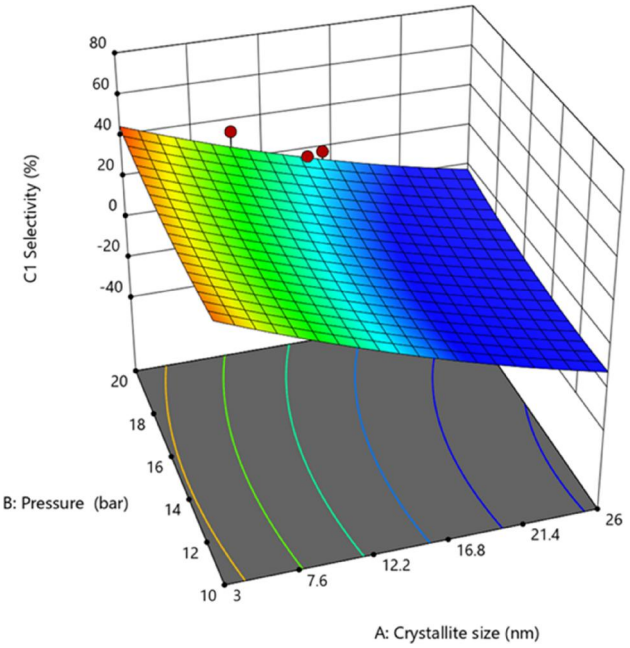



**Figure 3.** Three-dimensional (3-D) plot showing the effect of crystallite size and pressure on C1 selectivity (%). the 3-D plot was generated using design-expert 13. The red circles are data points above the predicted values, respectively.

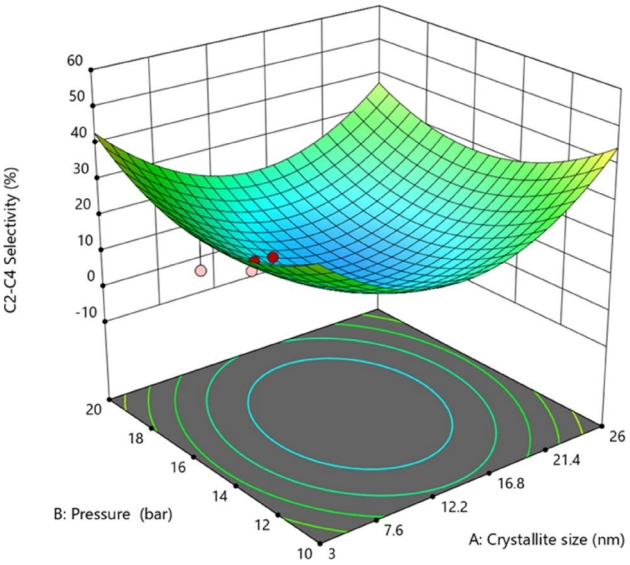



**Figure 4.** 3-D plot showing the effect of crystallite size and pressure on $C_2$–$C_4$ selectivity (%). The 3-D plot was generated using Design-Expert 13. The red and pink circles are data points above and below the predicted values, respectively.

crystallites of 21.4 to 26 are more selective to $C_2$-$C_4$ hydrocarbons. The data for this plot was extracted from various sources (Saib et al. 2002; Martínez et al. 2003; Song and Li 2006; Lira et al. 2008; Witoon et al. 2011).

The effect of pressure and crystallite size produced a dome-shaped distribution, contrary to

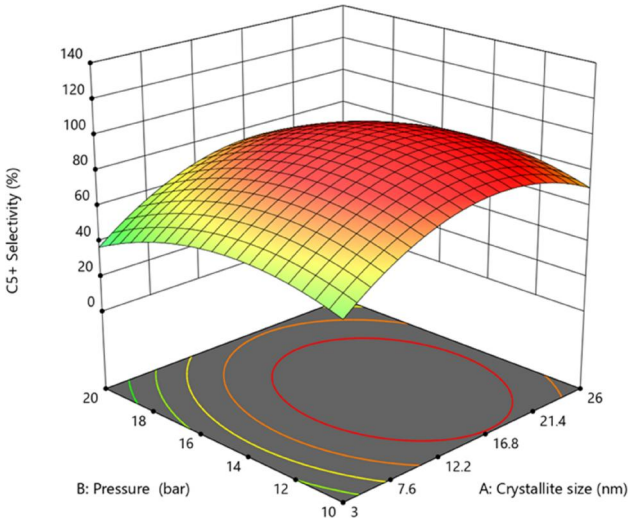



**Figure 5.** 3-D plot showing the effect of crystallite size and pressure on $C_{5+}$ selectivity (%). The 3-D plot was generated using Design-Expert 13.

the pattern observed for $C_2$-$C_4$ selectivity (on a carbon basis). Increasing pressure increased $C_{5+}$ to about 16 bar, then gradually decreasing until it reached 20 bar. $C_{5+}$ selectivity increased with an increase in crystallite size until 15.2 nm; it then decreased until it reached 26 nm. Analysis of the literature yielded Figures 3 to 5 (Saib et al. 2002; Martínez et al. 2003; Song and Li 2006; Lira et al. 2008; Witoon et al. 2011). Cobalt crystallite size appears to be an important factor that influences product distribution. This novel approach provides insight into selectivity being dependent on pressure and crystallite size in cobalt-catalyzed FTS.

In summary, maintaining the cobalt crystallite diameter within the specified range is crucial for optimizing FTS outcomes. This range ensures an optimal balance between catalytic activity, selectivity toward desired hydrocarbons, and resistance to deactivation mechanisms (to be discussed in the following section). Deviations from this range may lead to undesirable changes in CO turnover frequency and hydrocarbon selectivity, affecting the overall efficiency and performance of the Fischer-Tropsch synthesis process. Moreover, using unnecessarily large particle sizes also has these disadvantages (1) reduced active surface area since active sites for catalytic reactions are typically located on the surface of the catalyst; (2) diffusion limitations since large particles may tend to block the pores of the support material, and (3) large particles have a cost implication.

## Proneness of cobalt catalyst to oxidation

Cobalt catalyst oxidation has been studied extensively as a deactivation mode in FTS (Van Berge et al. 2000; Lira et al. 2008; Rytter and Holmen 2015; C. Kliewer et al. 2019; Choudhury et al. 2020; Okoye-Chine et al. 2023). The literature analysis suggests that, in general, the catalytic properties of small cobalt crystallite differ from that of larger ones in terms of activity, selectivity and deactivation. Table 1 shows that smaller Co particles are easily oxidized by the indigenous water vapor during FTS. A study done by Wang et al. (2012) concluded that with smaller Co crystallite (1.4–2.5 nm), the cobalt metal was easily oxidized by the indigenous water vapor, which led to reduced TOF and increased $CH_4$ selectivity. Wang et al. (2012) also observed that larger Co crystallites of 3.5–10.5 nm are immune to oxidation during FTS and do not affect TOF and $CH_4$ selectivity.

Thermodynamic analysis done by van Steen et al. (2005) showed that cobalt crystallites with a spherical shape and measuring $< 4.4$ nm in diameter are prone to oxidation during FTS ($P_{H2O}/P_{H2} < 1.5$, $T = 493$ K). The same qualitative observation was recorded by Iglesia (1997a), who reported rapid deactivation by oxidation during FTS of cobalt metal crystallite with a diameter of less than 5–6 nm. A high $P_{H2O}/P_{H2}$ ratio is needed to re-oxidize bulk cobalt metal, but these ratios are not encountered under normal FTS conditions (Iglesia 1997b; Hilmen et al. 1999; van Steen et al. 2005). High $P_{H2O}/P_{H2}$ ratios are possible at high per-pass conversions but the ranges of $P_{H2O}/P_{H2}$ ratios that may cause oxidation are not experienced in normal FT. The ratios of $P_{H2O}/P_{H2}$ experienced in normal FTS and $P_{H2O}/P_{H2}$ ratios required for oxidation are 3 and 123, respectively (van Steen et al. 2005). The thermodynamic feasibility of oxidizing small cobalt crystallites or forming an oxide shell may occur under conditions where the oxidation of bulk metallic cobalt is not feasible. This phenomenon is associated with the influence of surface energy on the overall process, which is lower for bulk

metal oxides compared to their corresponding bulk metals. Consequently, it is anticipated that nanosized crystals exhibit lower oxidation resistance compared to bulk crystalline materials.

Cobalt crystallite size significantly affects activation energy in stepwise reduction: $Co_3O_4 \rightarrow CoO \rightarrow Co^0$ [8] (Prieto et al. 2009). Thermodynamically, the oxidation of CoO by water during FTS is not favored as evidenced by a positive change in free energy (ΔG), indicating a non-spontaneous reaction, this is due to the weak reduction ability of $Co^0$ and the relatively feeble oxidizing potential of water. However, observations indicate that under a very low $P_{H2}/P_{H2O}$ ratio, where the partial pressure of hydrogen ($P_{H2}$) is much lower than the partial pressure of water vapor ($P_{H2O}$) in the gas phase, oxidation occurs (Van Berge et al. 2000). These conditions create circumstances in which the chemical potential of hydrogen is low, and the chemical potential of water is high. As a result, the oxidation of CoO by water moves toward equilibrium, despite being thermodynamically unfavorable.

Cobalt oxidation by $H_2O$ and $CO_2$ is governed by the $P_{H2}/P_{H2O}$ and $P_{CO}/P_{CO2}$ ratios in the reactor. Cobalt oxidation follows Equation (2) below.

$$Co(s) + \frac{1}{2}\ O_2(g) \Leftrightarrow\ CoO(s) \tag{2}$$

From Equation (2), the minimum oxygen partial pressure required to effect oxidation can be given by Equation (3):

$$\text{Log}\ P_{O2} - \log\ K(T) \tag{3}$$

For the oxidation of carbon monoxide (CO), it would be (Equation (4)):

$$CO(g) + \frac{1}{2}\ O_2(g) \Leftrightarrow\ CO_2(g) \tag{4}$$

The $O_2$ partial pressure can be given by Equation (5):

$$\text{Log}\ P_{O2} = 2\log\ (P_{CO2}/P_{CO})\ -\ \log\ Kco \tag{5}$$

Equation (6) can be used for the oxidation of hydrogen:

$$H_2(g) + \frac{1}{2}\ O_2(g) \Leftrightarrow\ H_2O(g) \tag{6}$$

The oxygen partial pressure can be given by Equation (7):

$$\text{Log}\ P_{O2} = 2\log\ (P_{H2}/P_{H2O}) + \log\ K_{H2} \tag{7}$$

The oxygen partial pressure corresponds to $P_{H2}/P_{H2O}$ and $P_{CO2}/P_{CO}$ ratios under certain conditions. The plot of $O_2$ partial pressure versus temperature with different partial pressures of $H_2$, $H_2O$, CO and $CO_2$ can be used to predict the stability of varying cobalt phases.

The parameters in Table 2 indicate that all the given reactions are thermodynamically feasible in the temperature ranges given. According to the three equations, the oxygen partial pressure can be related to $P_{H2}/P_{H2O}$ and $P_{CO2}/P_{CO}$ in the reactor at any point during the reaction. From the theoretical calculations of the thermodynamic properties, the oxidation of cobalt catalysts at different $P_{H2}/P_{H2O}$ and $P_{CO2}/P_{CO}$ ratios were plotted—see Figure 6 (The $P_{H2}/P_{H2O}$, $P_{CO2}/P_{CO}$ ratios correspond to a particular partial pressure of $O_2$.). The thermodynamic calculations for Co0 oxidation to $Co_3O_4$ are not presented, as they are approximately four orders of magnitude higher than for $Co^0$ to CoO.

The theoretical calculations show that it is impossible to oxidize a Co-based catalyst under normal FT conditions, as the $H_2O/H_2$ ratios are usually less than 10. This concurs with van Steen et al. (2005) calculations.This observation does not agree with many FT practitioners, who recorded catalyst oxidation after characterizing the spent catalyst. For our theoretical calculations to agree with the experimental data, the effects of crystallite size (that changes the surface energy of particles) on thermodynamic properties must be considered. (Here, crystallite size refers to the size of the cobalt metal clusters on the support surface.)

**Table 2.** Variation of thermodynamic parameters from 100 to 400 °C.

| | Thermodynamic parameters (range 100–400°C) | | |
|---|---|---|---|
| Equation | Log (Keq) | ΔH (kJ) | ΔG (kJ) |
| $Co(s) + \frac{1}{2}\ O_2(g) = CoO(s)$ | 58.34 to 28.94 | −473.83 to -468.00 | −416.70 to -372.85 |
| $H_2(g) + \frac{1}{2}\ O_2(g) = H_2O(g)$ | 63.04 to 32.64 | −485.13 to -490.55 | −450.33 to -420.54 |
| $CO(g) + \frac{1}{2}\ O_2(g) = CO_2(g)$ | 70.18 to 34.80 | −566.70 to -567.05 | −501.30 to -448.40 |

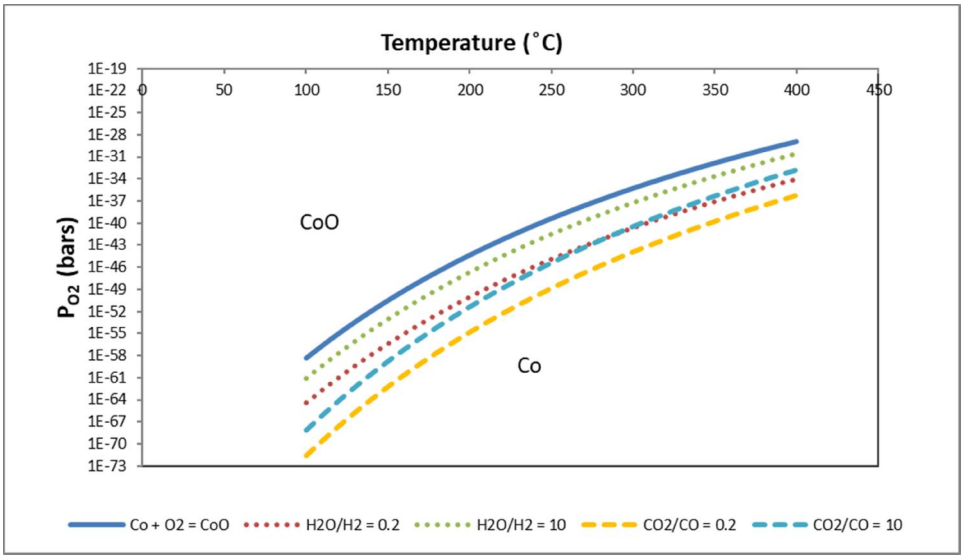



**Figure 6.** Theoretical study of the effect of $P_{H2O}/P_{H2}$ and $P_{CO2}/P_{CO}$ on cobalt catalyst oxidation.

As per Table 1, activity and selectivity can change with changes in crystallite size. Oxidation of cobalt only happens with substantial $P_{H2O}/P_{H2}$ ratios, and these ratios are not encountered under normal FTS conditions as stated earlier. The literature analysis done by Van de Loosdrecht et al. [39] revealed that, with FTS, $PH_2$ ranges from 6.5 to 9.2 bar, and a $P_{H2O}$ between 4.6 and 7.6 bar, which corresponds to a $P_{H2O}/P_{H2}$ ratio between 0.5 and 1.2. Cobalt particles of less than 4–5 nm are oxidized if the $H_2O/H_2$ ratio is 1–1.5 (van Steen et al. 2005). Schanke et al. (1995) observed no oxidation on 15 and 25 nm particles at a $P_{H2O}/P_{H2}$ of 0.33. Hilmen et al. (1999) experimented with 10 and 16 nm particles using a $P_{H2O}/P_{H2}$ ratio of 10 and observed no Co oxidation. Bian et al. (2003) studied larger Co-crystallites (10 and 29 nm) using a high $P_{H2O}/P_{H2}$ of 6.11 and observed no oxidation. A cobalt particle smaller than 4 nm oxidized at a $P_{H2O}/P_{H2}$ ratio of 0.74 (Iglesia 1997a). A study done by Jacobs et al. (2003) on a 6 nm Co particle showed that a $P_{H2O}/P_{H2}$ ratio of 0.56 resulted in no oxidation, whereas a $P_{H2O}/P_{H2}$ of 0.60 resulted in oxidation. Therefore, cobalt oxidation of crystallites less than 6 nm can be avoided by ensuring the correct combination of reactor partial pressures of $P_{H2O}$ and $P_{H2}$.

A study done by Lu (2011) on FT product distribution (using 10%C0/$TiO_2$) resulted in different $P_{H2O}/P_{H2}$ ratios when using a continuously stirred tank reactor (CSTR) and tubular fixed-bed reactor (TFBR) at $H_2/CO = 2$ and 20 bar and different pressure levels. In the same study, it was shown that the $P_{H2O}/P_{H2}$ ratio increases with temperature. With a TFBR, the ratios are significantly higher than with a CSTR. When using a CSTR, the proportions are comparatively lower and tend to approach an asymptote as the temperature increases toward 240 °C. The distribution of FT products is influenced by several parameters, including the type of reactor employed thus affecting the $P_{H2O}/P_{H2}$ ratio. The impact of temperature on the FT product distribution may vary between the Fixed Bed Reactor (FBR) and the Continuous Stirred Tank Reactor (CSTR) due to the inherent characteristics of these reactors. The Anderson-Schulz-Flory (ASF) model suggests that the distribution of FT products conforms to a geometric distribution, with a chain growth probability factor ($\alpha$) that declines with an increase in temperature. As a result, higher temperatures tend to promote the formation of lighter hydrocarbons, such as methane and ethane, while lower temperatures favor the production of heavier hydrocarbons, such as waxes and diesel. The model for the ASF synthesis serves as an elementary representation of the FT synthesis. It omits the secondary reactions that occur within the reactor, such as cracking, isomerization, hydrogenation, and water-gas shift. These reactions can significantly impact the FT product distribution, causing it to differ from the ideal ASF distribution. For instance, the process

of cracking can break down long-chain hydrocarbons into shorter ones, isomerization can alter the structure of the hydrocarbons from linear to branched, hydrogenation can decrease the olefin content, and water-gas shift can consume CO and $H_2O$ while producing $CO_2$ and $H_2$.

The extent of secondary reactions in chemical reactors is influenced by the reactor type and operating conditions. FBRs experience temperature variations influenced by factors such as heat transfer, reaction kinetics, and reactant concentration. This enhances the rate of secondary reactions, such as cracking and isomerization, leading to a more diverse and complex distribution of products. Conversely, in CSTRs, catalyst particles are well-mixed, resulting in a more uniform temperature. As a result, secondary reactions occur at a lower rate, yielding a more predictable and consistent product distribution. The CSTR exhibits little variation in $pH_2O/PH_2$ with an increase in reaction temperature, and this could be attributed to the fact that the CSTR has a lower rate of secondary reactions than the FBR, making it less sensitive to temperature changes.

## The effect of cobalt–support interaction

In studying the effect of cobalt crystallite, Bezemer et al. (2006) opined that these types of experiments are better carried out using inert materials such as graphitic or carbon-based supports. Oxidic supports, silica and alumina tend to form mixed oxides that are not reduceable - such as cobalt aluminate or cobalt silicate - which may affect the observations (Van Berge et al. 2000; Li et al. 2002; Wolf et al. 2021). The strength of cobalt–support interaction has been found to increase in the order $SiO_2 < Al_2O_3 < TiO_2$ (Jacobs et al. 2007; James and Maity 2016; Kliewer et al. 2019; Petersen et al. 2019; Yan et al. 2021). Deductions from the literature indicate that strong Co–support interaction of $Al_2O_3$, and particularly $TiO_2$, results in increased dispersion and there is a tendency to form cobalt aluminates and titanates, respectively. This affects the density of the $Co^0$ surface sites. Comparatively speaking, the interaction of cobalt on silica support is weaker, which is ideal for complete cobalt oxide reducibility. However, there is a problem with the agglomeration of cobalt crystallites during catalyst preparation, which also happens at high temperatures during calcination (Martínez et al. 2003). This sintering leads to low Co crystallite dispersion.

## Crystallite size measurement techniques

The characterization of crystallites involves a range of techniques for determining their size, morphology, and structure. Among the most commonly used methods, X-ray diffraction (XRD) allows for the analysis of crystal structure and the determination of lattice parameters, as well as peak broadening, which can provide indications of crystallite size. Transmission electron microscopy (TEM), on the other hand, provides high-resolution imaging of individual crystallites, revealing information about their shape, size, and defects. Scanning electron microscopy (SEM) is a useful method for obtaining surface morphological information. In addition, techniques such as atomic force microscopy (AFM) and dynamic light scattering (DLS) can be employed to study the size and shape of crystallites.

Transmission electron microscopy (TEM), X-ray diffraction (XRD) and $H_2$-chemisorption are often employed to measure crystallite size before running FTS. These analytical techniques often show consistency with crystallite sizes (Miller et al. 1993; Schanke et al. 1995; Jacobs et al. 2003; Bezemer et al. 2006; Den Breejen et al. 2009; Saib et al. 2010) with X-ray absorption studies giving results that are within the experimental error. Powder XRD has been reported to measure millions of crystals and provide the precise size distribution of nanomaterials (Chauhan and Chauhan 2014). The terms particle size and crystallite size are often used interchangeably to mean the same thing, but these refer to two distinct properties of a material. Particles comprise of several small crystallites, and nanomaterial properties depend and comprise several small crystallites, and nanomaterial properties depend on crystallite size, not particle size (Chauhan and Chauhan 2014).

Due to the principle of measurement, crystallite size calculated with XRD is always smaller than when using the chemisorption method. This

is expected because the XRD measurements also record dislocations in the crystal structure that are not registered by chemisorption (Geyer et al. 2012). The crystallite size given by TEM analysis agrees with the size derived from XRD (Rozita et al. 2010). Usually, in a minimal particle size regime (nanometer scale), there is close agreement between the TEM and XRD measurements. However, for larger particle size regimes, TEM tends to provide a comparatively larger average particle size than XRD. The discrepancy is attributed to the size that is determined by XRD correlating with the average of the smallest undistorted regions in the material. In contrast, TEM measurements relate to scanned areas separated by more-or-less sharp contours in the micrograph (Rozita et al. 2010).

### Characterization of cobalt crystallite size

In FTS, precision catalyst development with defined crystallite size is an area of interest that researchers continue to look at. From the previous sections, it is clear that knowledge of the crystallite size distribution is crucial for interpreting the experimental results of FTS. Various synthetic pathways have been adopted for the preparation of catalysts with good uniform dispersion and controlled crystallite size. Examples include incipient wetness impregnation (Xiong et al. 2005; Song and Li 2006; Lira et al. 2008; Fu et al. 2014; Gavrilović et al. 2018; Rytter et al. 2018); the sol-gel technique (Okabe et al. 2004; Liu et al. 2010; Bykova et al. 2012; Sukkathanyawat et al. 2015); the chemical deposition method (Kazemnejad et al. 2019); the precipitation method (Li et al. 2017); and the impregnation method (Bian et al. 2003). A review by Ghogia et al. (2021) provides an overview of these methods along with a detailed description of each. Different characterization techniques are used to measure crystallite size accurately. The techniques include TEM, XRD and $H_2$-chemisorption as stated earlier. Each technique has certain advantages and disadvantages, as there are limitations, given that they are prone to operational and other fundamental uncertainties. So, it is recommended that more than one technique is used to verify the agreement of the data. Agreement of the data, which is determined using various methods, proves the absence of significant errors in the methods used for each supported metal catalyst. After analyzing various experiments conducted to determine crystallite sizes using the XRD Scherrer formula and TEM, it was concluded that both methods yield similar crystallite size values, especially for sizes smaller than 60 nm (Vorokh 2018). Thus, a combination of at least two methods is needed to determine catalyst crystallite size accurately.

### TEM application in determining crystallite size

TEM has been applied to image crystallite size directly on the supported catalyst. However, for accuracy and reproducibility, there is a need for accurate crystallite size distribution analysis. TEM has the advantage of the real-space visualization of nanoparticles. Nevertheless, to ensure accurate results, the operator must still select the correct magnification and have reasonable choices regarding the type of imaging (bright vs dark field), method of analysis, and a manual or automated method (Pyrz and Buttrey 2008). These choices have an impact on resolution, the contrast between the background and the particles, the particle population in each image, the efficiency of the analysis and proper background-particle boundary determination (Pyrz and Buttrey 2008). It is important to note that images visualized at coarse magnifications clearly show all the particles in that given area, but the reliability of the quantification was severely limited, as high magnification imaging results in sampling fewer particles. This limitation contributes to errors or bias in determining the crystallite size of a given sample. Therefore, the statistical significance of the crystallite size determination will be compromised if the particle population is not captured and it is not representative of the particle population. Therefore, all variables should be considered, in order to measure particle size distribution with statistical significance and accuracy.

### TEM limitations

Generally, measuring the crystallite diameter on the supported catalyst and understanding the

distribution using TEM can be a challenging exercise. To obtain statistically meaningful data from TEM, many points should be analyzed, many particles should be analyzed and many crystallites should be measured. Other challenges with TEM image analysis are the presence of crystallites as clusters at different heights; crystallites that are sometimes embedded in support material; crystallites that overlap; and an uneven background. In order to address these issues, Gontard et al. (2011) invented an image-processing algorithm to assist in measuring crystallite size and their distribution using TEM images. The algorithm reportedly allows crystallites to be detected and characterized with greater accuracy than when using other conventional methods. In another study, Fisker et al. (2000) developed an automated image analysis technique built on a deformable ellipse model to accurately and robustly estimate crystallite size distribution from thousands of crystallites. This method has also proved to be very useful.

Figure 7 shows synthesized uniform-sized cobalt crystallites on mesoporous $SiO_2$ supports. The number of crystallites varies per given area at the same magnification. There is a correlation between crystallite size and selectivity, so the ability to tune the crystallite size controls the selectivity of the products. However, a correlation between shape and product selectivity is not mentioned in the available literature. Another, disadvantage of TEM is sometimes a lack of contrast between crystallites and the support, and it is difficult to see tiny particles of 0.5 nm (Mustard and Bartholomew 1981). In principle, TEM can measure the size of a discrete particle, which can be used to determine the average particle size. However, different points or locations need to be imaged to avoid bias and the pictures studied should be representative of the whole sample.

### X-ray diffraction (XRD)

XRD is another technique that is often used to measure the mean size of crystallites by applying the Scherrer equation to XRD data. The history of applying the Scherrer equation in determining crystallite size is documented in articles written by Alexander and Klug (1950), and Langford and Wilson (1978). The Scherrer equation is the most commonly used modus operandi in FT reported in the literature for extracting crystallite size

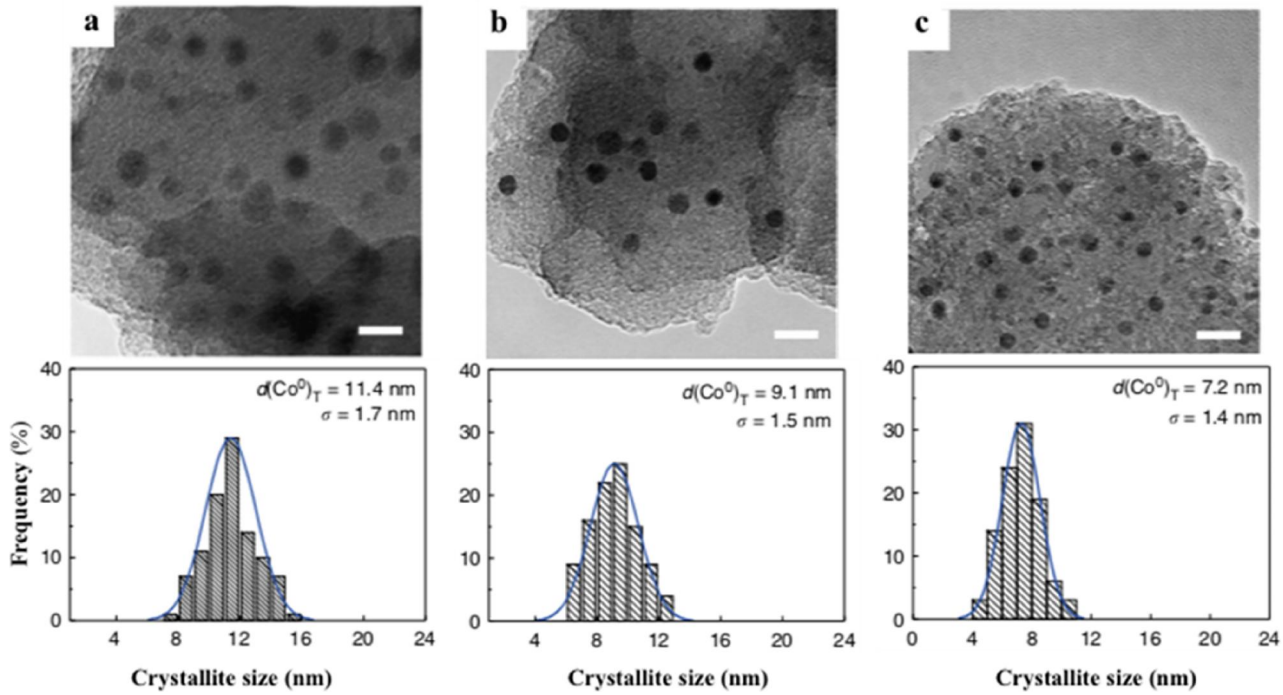



**Figure 7.** Images obtained from TEM and a reduced catalyst's corresponding cobalt crystallite size distribution. Crystallite size decreases from a > b > c, and metallic cobalt crystallites are dispersed almost homogeneously with a narrow size distribution. The figure was modified with permission from (Cheng et al. 2018).

information from XRD data. The Scherrer Equation was formulated in 1918 to compute the diameter of crystallite. It is given in Equation (8).

$$L = \frac{K\lambda}{\beta.\cos\theta} \tag{8}$$

Where L is the average crystallite size (crystallite diameter in nanometer (nm)); K is the crystallite shape-related constant, normally taken as 0.9 (depending on the shape of the crystallite); $\lambda$ is the wavelength of the X-ray, usually in nm; $\beta$ is the Full Width at Half Maximum (FWHM) at $2\theta$ in radians ($\beta$ = value of FWHM X $\pi/180$), and $\beta$ varies inversely with crystallite diameter (L); $\theta$ is the Bragg angle for the peak at $2\theta$ (in degrees); $\theta$ = ($2\theta/2$) FWHM, and $\theta$ can be expressed in radians or degrees, since the value of Cos$\theta$ corresponds to the same value (Monshi et al. 2012).

### *Uncertainties in calculating crystallite size*

The accuracy of the familiar Scherrer Equation is limited by the uncertainties in K (the crystallite shape factor) and $\beta$ (the pure diffraction broadening) (Alexander and Klug 1950). In reality, crystallites are not usually uniformly perfect but have irregular shapes. However, the Scherrer Equation assumes a regular shape for all samples. Although crystallite shape is usually irregular, shapes are often approximated as spheres, triangular prism, cubes, tetrahedrons and octahedrons, and in some cases include shapes that do not have cubic symmetry (Lele and Anantharaman 1962; Wilson 1969; Louër et al. 1972). Special cases of non-cubic symmetry crystallite shapes that have been considered are parallelepipeds such as needles and plates (Langford and Wilson 1978).

The K value depends on the determined width, crystallite shape and distribution of the size. The values often used for K (the shape factor) are 0.94 for crystallites that are spherical and 0.89 for other shapes. These values can be approximated to be 1 after rounding off. K varies from 0.62 to 2.08. A detailed discussion of K is given by Langford and Wilson (1978). The literature survey shows that, when using the Scherrer Equation, the estimates are usually that crystallites are spherical; however, prior analysis using other methods (TEM, SEM, and AFM) to determine the average crystallite shape can assist in determining the most accurate value of K.

The accuracy of Equation (8) (the Scherrer crystallite size equation) is restricted partly by the uncertainty regarding the $\beta$ value, which varies inversely with crystallite size (Alexander and Klug 1950). FWHM is defined as the diffraction peak width, in radians, at a height halfway between the base and the maxima of the peak (Muniz et al. 2016). FWHM of the broadened line has been criticized for giving unreliable crystallite size values. Therefore, it was proposed that the integral breadth be used together with the Scherrer equation to reduce errors in determining crystallite size (Bushroa et al. 2012). Moreover, the line shape of an XRD pattern is affected by the uneven distribution of crystallite and the wide distribution of size (Bushroa et al. 2012). The Scherrer formula has a lower limit of applicability, which has been established. It has been shown that the error when using the Scherrer formula non-linearly increases with a crystallite size of less than 4 nm (Vorokh 2018). In another study, XRD was reported to be insensitive to low metal loading and small particles (<3 nm) (Mustard and Bartholomew 1981).

### *Crystallite definition*

Here, the phrases crystallite size and particle size, and the word size are synonymous with the diameter of the crystallite, with the diameter being defined as the length of a straight line traversing through the middle of the mass of the crystallite and ending at the crystallite boundary (Green 1927; Heywood 2010). For non-uniform crystallite that cannot be completely defined by a single mean value, a mathematical shape factor for defining the geometric shape can be applied if accuracy is important (Hatch 1933). Several definitions of particle size exist in the literature, but the most appropriate is governed by the system being examined and the analysis technique employed (Matyi et al. 1987). For instance, XRD is sensitive to the crystallite size on the surface or inside any given particle. However, the phrase crystallite size seems more accurate, since individual particles can be made up of many crystallites or domains with a non-identical orientation. This distinction is significant if the diameter measured from diffraction broadening is juxtaposed with that obtained using other methods.

Figure 8 shows that an increase in the size of particles tends to result in the narrowing of the peaks to resemble a coarse crystalline material. Smaller particles less than 1.5 nm tend to produce broad peaks synonymous with amorphous substances (Vorokh 2018). This phenomenon is observed even if the particles or crystallites are not the same shape and size. The peak width varies with particle or crystallite size, and a narrow peak corresponds with a bigger crystallite diameter. When the peaks are broader, there is a limit to the smallest nanoparticles that can be measured by XRD, (<3 nm) (Mustard and Bartholomew 1981).

### *H2 chemisorption*

Many catalyst characterization studies have used $H_2$ chemisorption as a crystallite size measuring technique (Bezemer et al. 2006; Den Breejen et al. 2009; Prieto et al. 2009; Rane et al. 2012). $H_2$ chemisorption measurements relate the consumption of $H_2$ gas molecules to the available surface area of the supported metal crystallites. The relationship that exists between $H_2$ consumption and the exposed surface area is governed by the chemisorption stoichiometry of the hydrogen-to-metal atom. This technique is useful for small particles when the size is difficult to estimate through electron microscopy or XRD (Almithn and Hibbitts 2018). The approximation of active crystallite size calculation is a geometrical assumption that is based on the shape of the crystallite having a regular geometry, with the ideal geometry being a sphere (Webb 2003).

This analysis makes use of an expression of grain geometry. Using the approximated regular geometry, the size (being the diameter) can then be computed in terms of volume and area (Webb 2003). The diameter computed is the average diameter of the active crystallite onto which hydrogen adsorption occurred. The significant economic advantages of using $H_2$ chemisorption in measuring particle size are that it is less expensive than TEM and XRD techniques, is fairly accurate, and measures particles of all sizes. However, it has disadvantages, as it is easily affected by contamination, there is metal support interaction and adsorption stoichiometry could vary with dispersion or metal loading (Mustard and Bartholomew 1981). The $H_2$ chemisorption method also has other inherent difficulties that hinder its effective application, for example, in order for measurement by $H_2$ chemisorption to make sense, the probe gas should be adsorbed on the surface of the metal as a monolayer and gas desorption should be complete (Matyi et al. 1987).

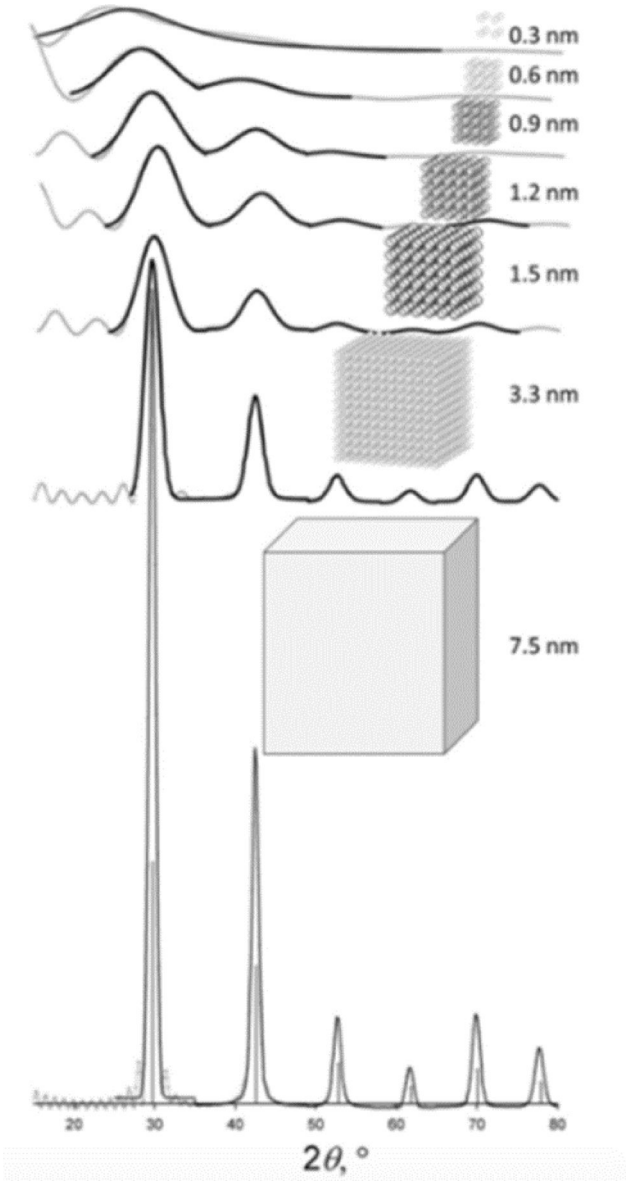



**Figure 8.** Diffraction curves of model particles with a cubic shape and a cubic unit cell structure. Particle size measurements are given in nm (Vorokh 2018).

### *Cobalt crystallite size determined by TEM, $H_2$ chemisorption and XRD*

The crystallite sizes of cobalt-based catalysts are tabulated in Table 3. Various authors employed different preparation methods for the catalysts,

and distinct analytical techniques (TEM, H2 chemisorption, and XRD) were utilized to determine the crystallite size. In comparing and computing differences obtained by using two or more methods for crystallite size determination, a statistical approach was employed to check for variations when specific techniques were applied. One-way ANOVA followed by post-hoc Bonferroni correction was used to analyze the results obtained from the literature.

Table 4 summarizes the one-way ANOVA results that compare different analysis methods used to determine crystallite size. A post-hoc Bonferroni correction test was performed to enable a comparison of the different techniques, and the results are tabulated. As shown in all the ANOVA tables, the P values are greater than 0.05 and F is less than Fcritical, which provides strong evidence that the techniques yield almost similar measurements.

A one-way ANOVA, followed by a post-hoc Bonferroni correction test, indicated that any of the techniques (TEM, XRD and $H_2$ chemisorption) can be used to determine crystallite size with P(T <=t) two-tail values that are greater than an alpha value of 0.05, even after applying the Bonferroni test (all are above 0.01666667). Any of the techniques discussed can be adopted to give measurements that are of statistical significance, as there are no differences within groups or any combination of techniques.

## Cobalt catalyst reduction

Temperature-programmed reduction (TPR) is a technique applied in FT catalysis, with a catalyst precursor undergoing monitored reduction while the temperature is increased linearly with time. TPR studies of catalysts are a crucial step in FT technology as they produce the active catalyst. The method has been used extensively to study supported and unsupported catalysts, to extract qualitative information such as the oxidation state of the reducible species present (Jacobs et al. 2007; Jozwiak et al. 2007; Bao et al. 2009; Gorimbo 2018). The technique is highly sensitive to the presence of species in a reducible form and discussions on the sensitivity of the TPR profiles (peak shape, maximum temperature, resolution of reduction steps, etc.) have been published (Bosch et al. 1984; Malet and

**Table 3.** Cobalt crystallite size determined by TEM, $H_2$ chemisorption and XRD.

| | Crystallite determination method (measurements in nm) | | | |
|---|---|---|---|---|
| Co- based catalyst | TEM | $H_2$ chemisorption | XRD | References |
| $Co/SiO_2$-20 | 26 | 19.8 | – | (A. M. Saib et al. 2002) |
| $Co/SiO_2$-40 | 3 | 5.9 | – | |
| $Co/SiO_2$-60 | 6.7 | 6 | – | |
| $Co/SiO_2$-100 | 6.9 | 7.3 | – | |
| $Co/SiO_2$-150 | 8.3 | 10.6 | – | |
| Co-silica ID | – | 19.9 | 23.5 | (Zhang et al. 2006) |
| Co-acetic acid | – | 14.2 | 16.1 | |
| Co-ethanol | – | 19 | 22.3 | |
| Co-1-propanol | – | 15.6 | 18.2 | |
| Co-1-butanol | – | 14.9 | 16.5 | |
| 30% $Co/SiO_2$ | 183 | 141 | 125 | (Prieto et al. 2009c) |
| 10% Co/ITQ(1) | 12.8 | 10.4 | 12.5 | |
| 10% Co/ITQ(2) | 8.2 | 8.9 | 9.9 | |
| 10% Co/ITQ(3) | – | 7.3 | 9.1 | |
| 10% Co/ITQ(4) | 6.3 | 5.6 | 6.8 | |
| 10% Co/ITQ(5) | – | – | 5.9 | |
| Cat-12 h | 11.4 | 10.6 | 12.8 | (Cheng et al. 2018) |
| Cat-8h | 9.1 | 8.9 | 11 | |
| Cat-4h | 7.2 | 7.3 | 8.9 | |
| Cat-1M | 14.3 | 12.3 | 13.1 | |
| HDP11 | 30 | 25 | | (G. Leendert Bezemer et al. 2006) |
| HDP9 | 14 | 12.5 | | |
| IWN13 | 7.5 | 8.5 | | |
| IEN4 | 3.6 | 4.4 | | |
| IWA1 | 3.7 | 6.1 | | |
| 5Co/M | 3 | – | 5 | (Li et al. 2006) |
| 10Co/M | 4.5 | – | 11 | |
| 15Co/M | 6.5 | – | 14 | |

**Table 4.** Analysis of variance (ANOVA): single factor.

Summary

| Groups | Count | Sum | Average | Variance |
|---|---|---|---|---|
| TEM vs $H_2$ Chemisorption | 18 | 72.1 | 4.00555556 | 92.5923203 |
| TEM vs XRD | 11 | 82.7 | 7.51818182 | 285.787636 |
| XRD vs $H_2$ Chemisorption | 14 | 41.8 | 2.98571429 | 14.6551648 |

ANOVA

| Source of variation | SS | df | MS | F | P-value | F crit |
|---|---|---|---|---|---|---|
| Between groups | 136.483561 | 2 | 68.2417803 | 0.59052311 | 0.55879474 | 3.23172699 |
| Within groups | 4622.46295 | 40 | 115.561574 | | | |
| Total | 4758.94651 | 42 | | | | |

t-Test: Two-sample assuming equal variance

| | TEM vs $H_2$ chemisorption | TEM vs XRD | | |
|---|---|---|---|---|
| Mean | 4.00555556 | 7.51818182 | | |
| Variance | 92.5923203 | 285.787636 | | |
| Observations | 18 | 11 | | |
| Pooled variance | 164.146141 | | | |
| Hypothesized mean Difference | 0 | | | |
| df | 27 | | | |
| t Stat | −0.7163911 | | | |
| P(T<=t) one-tail | 0.2399505 | | | |
| t Critical one-tail | 1.70328845 | | | |
| P(T<=t) two-tail | 0.47990099 | | 0.01666667 | FALSE |
| t Critical two-tail | 2.05183052 | | | |

t-Test: Two-sample assuming equal variance

| | TEM vs $H_2$ chemisorption | XRD vs $H_2$ chemisorption | | |
|---|---|---|---|---|
| Mean | 4.00555556 | 2.98571429 | | |
| Variance | 92.5923203 | 14.6551648 | | |
| Observations | 18 | 14 | | |
| Pooled variance | 58.8195529 | | | |
| Hypothesized mean Difference | 0 | | | |
| df | 30 | | | |
| t Stat | 0.37316165 | | | |
| P(T<=t) one-tail | 0.355826 | | | |
| t Critical one-tail | 1.69726089 | | | |
| P(T<=t) two-tail | 0.711652 | | 0.01666667 False | FALSE |
| t Critical two-tail | 2.04227246 | | | |

t-Test: two-sample assuming equal variance

| | TEM vs XRD | XRD vs $H_2$ chemisorption | | |
|---|---|---|---|---|
| Mean | 7.51818182 | 2.98571429 | | |
| Variance | 285.787636 | 14.6551648 | | |
| Observations | 11 | 14 | | |
| Pooled variance | 132.538848 | | | |
| Hypothesized mean Difference | 0 | | | |
| df | 23 | | | |
| t Stat | 0.97713251 | | | |
| P(T<=t) one-tail | 0.16933498 | | | |
| t Critical one-tail | 1.71387153 | | | |
| P(T<=t) two-tail | 0.33866996 | | 0.01666667 | FALSE |
| t Critical two-tail | 2.06865761 | | | |

Bonferroni post hoc test.

Caballero 1988; Fierro et al. 1994; Christel et al. 1997; Giordano et al. 2000).

The TPR technique has been used as a successful fingerprint method for characterizing FT catalysts - mainly cobalt and iron. This section focuses on the cobalt-based catalyst in FTS only. Several factors that influence the TPR profile have been studied, and sample weight, hydrogen concentration, carrier flow rate, total hydrogen consumption, and heating rate tend to have a greater degree of influence (Bosch et al. 1984). The conditions reported in the literature differ

widely; as a result, it is challenging to compare TPR profiles obtained by different researchers (Figure 9).

TPR with hydrogen is a commonly used technique for characterizing catalysts in FTS reactions. An in-depth understanding of the accurate reduction pathway of the FTS catalyst is an important piece of information. In the case of the cobalt-based catalyst, $Co_3O_4$ undergoes reduction to Co in two steps, with CoO being the intermediate species regardless of support type ($SiO_2$, $TiO_2$, and $Al_2O_3$) (Xiong et al. 2005; Jacobs et al. 2007; Kliewer et al. 2019). Using hydrogen ($H_2$) as the reduction gas yields two different reduction regions, as shown in Figure 9.

Various reducing agents have been used in FTS, including hydrogen, CO and syngas (Gorimbo 2016). In the case of hydrogen, the degree of reduction is determined by monitoring $H_2$, consumption while increasing the sample temperature at a constant rate. As a result, the reduction profiles are obtained at different temperatures. An elevated temperature is sometimes necessary for reduction, such as when strong metal-support interaction is experienced (Jacobs et al. 2007).

The stoichiometry of Equation (9) suggests that 1 mole of $Co_3O_4$ yields 4 moles of $H_2O$ during reduction.

$$H_2\text{–reduction}: Co_3O_4 + 4H_2 \rightarrow 3Co + 4H_2O,\ \Delta H = -57.1\ \text{kJ/mol};\ \Delta G = -140.4\ \text{kJ/mol} \quad (9)$$

$Co_3O_4$ reduction to CoO consumes 1 mole of hydrogen and then reduces to metallic Co using

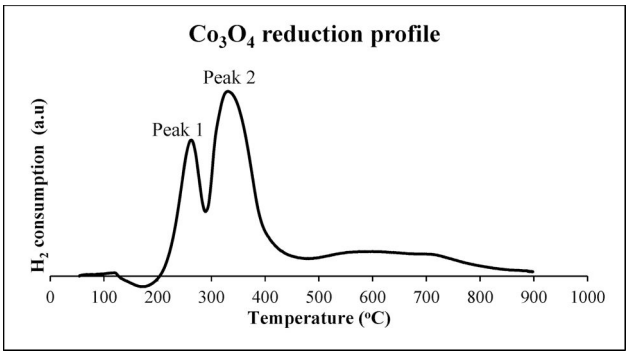



**Figure 9.** The pattern represents the TCD signal resulting from $Co_3O_4$ reduction in hydrogen for a cobalt-based catalyst (Gorimbo et al. 2020).

1 mole of $H_2$ - see Figure 10.

$$\text{First peak}: Co_3O_4 + H_2 \rightarrow 3CoO + H_2O,\ \Delta H = -3.93\ \text{kJ/mol};\ \Delta G = -14.4\ \text{kJ/mol} \quad (10)$$

$$\text{Second peak}: CoO + H_2 \rightarrow Co + H_2O,\ \Delta H = -12.0\ \text{kJ/mol};\ \Delta G = -43.2\ \text{kJ/mol} \quad (11)$$

### *Thermodynamics of Co-based catalysts reduction*

Gibbs free energy and enthalpy of the reaction system at specific temperature and pressure levels have been used to plot the mass balance-attainable region of the FT system (Gorimbo et al. 2020), while standard energies are provided in Equations 9–11. Gibbs free energy gives the work potential of the given scenario, while enthalpy presents the minimum reaction energy requirements of the system. So, +ΔH values indicate that work and energy should be supplied to the reaction system, whereas -ΔH values indicate that work and energy are released by the system. Pressure deviations are not considered significant in terms of enthalpy and Gibbs free energy at the temperature levels studied.

$$\Delta H^0 = \Delta H_0^0 + R\int_{T_0}^{T} \frac{\Delta C^0}{R} dT \quad (12)$$

Where $\Delta H^0$ and $\Delta H_0^0$ are heat of formation of the components at temperature T and reference temperature $T_0$. The heat capacity term at temperature T is given by Equation (13).

$$\frac{\Delta C_P^0}{R} = A + BT + CT^2 + DT^{-2} \quad (13)$$

Where A, B, C, and D are heat transfer coefficients. Integrating Equations (11) and (12) to get $\Delta H^0$ at temperature T gives Equation (13), where $\Upsilon = \frac{T}{T_o}$

$$\Delta H^\circ = \Delta H_o{}^\circ + R*\left[\Delta A*T_o*(\Upsilon-1) + \frac{\Delta B}{2}*T_o{}^2\ *(\Upsilon^2-1) + \frac{\Delta C}{3}*T_o{}^3\ *(\Upsilon^3-1) + \frac{\Delta D}{T_o}*\left(\frac{\Upsilon-1}{\Upsilon}\right)\right] \quad (14)$$

ΔG at various temperatures can be calculated using Equation (14). (15) (Smith et al. 2018).

$$\Delta G^{\circ}T = \Delta H^{\circ}_{o-}\frac{T}{T_o}\left(\Delta H^{\circ}_{o-}\ \Delta G^{\circ}o\right) + R\int_{T.}^{T}\frac{\Delta Cp^{\circ}}{R}dT - RT\int_{T.}^{T}\frac{\Delta Cp^{\circ}}{R}\frac{dT}{T} \quad (15)$$

where $\int_{T.}^{T}\frac{\Delta Cp^{\circ}}{R}dT = \Delta A*T_o*(\tau - 1) + \frac{\Delta B}{2}* \frac{\Delta B}{2}*T_o{}^2*(\tau^2 - 1) + \frac{\Delta}{3}*T_o{}^3*(\tau^3 - 1) + \frac{\Delta D}{To}*\left(\frac{\tau-1}{\tau}\right)$ and $\int_{T.}^{T}\frac{\Delta Cp^{\circ}}{R}\frac{dT}{T} = \Delta A*ln\tau + [\Delta BT_o + \left(\Delta CT_o{}^2 + \frac{\Delta D}{\tau^2 T_o{}^2}\right)\left(\frac{\tau+1}{2}\right)]*(\tau - 1)$

(Gorimbo et al. 2020) applied the Attainable Region (AR) approach to cobalt catalyst reduction thermodynamics using the above equations and depicted the reduction pathway, as shown in Figure 10. The method entails setting up ideal conditions for Co reduction and focusing on determining minimal G at varying temperatures. Figure 10, supported by Figure 9 and TAR space diagrams, shows that the reduction of $Co_3O_4$ often happens through two reaction stages. Peak 1 is assigned to direct reduction of $Co_3O_4$ to Co and $Co_3O_4$ to intermediate CoO. Then peak 2 is assigned to the reduction of $Co_3O_4$ to Co or CoO to Co (Jacobs et al. 2007).

## Pore size effect on crystallite sizes

Several catalysts used in FTS are porous, with pores grouped as macropores, mesopores and micropores (Haber 1991). The surface area, pore volume and pore diameter determined using the Brunauer, Emmett and Teller (BET) theory, influences catalyst activity and product selectivity. These parameters govern reactant diffusion. Porosity relates to the volume percentage occupied by the pores, and the pore-size distribution refers to the pore volume distribution with reference to pore size. Porosity is a key factor in controlling the diffusion of reactants from the pore mouth through the catalyst pores to the immediate vicinity of the internal catalytic surface and the desorption of the products from the surface (Haber 1991).

The metal crystallite size and the extent of reduction were shown to increase linearly with an increase in the support pore diameter (Iglesia 1997a). Iglesia (1997a) also observed that the metal crystallites form clusters on the surface of the support and that increasing the support pore diameter resulted in an increase in the size of the clusters (Iglesia 1997a). If cobalt crystallites formed are bigger than the average pore diameter of the support, they will probably be situated on the external surface of the support. A general observation is that cobalt crystallite distribution on the support is not even, i.e. clusters of various-sized crystallites can be observed on the support (Saib et al. 2002).

Xie et al. (2012) used carbon nanotubes (CNT) and reported an important phenomenon: Co catalyst crystallites inside CNT reduced more easily than those outside CNT; with crystallites inside the CNT, smaller Co crystallites reduced better than bigger crystallites. Xie et al. (2012) observed that FT catalytic activity was higher for Co crystallite inside the CNT than outside it.

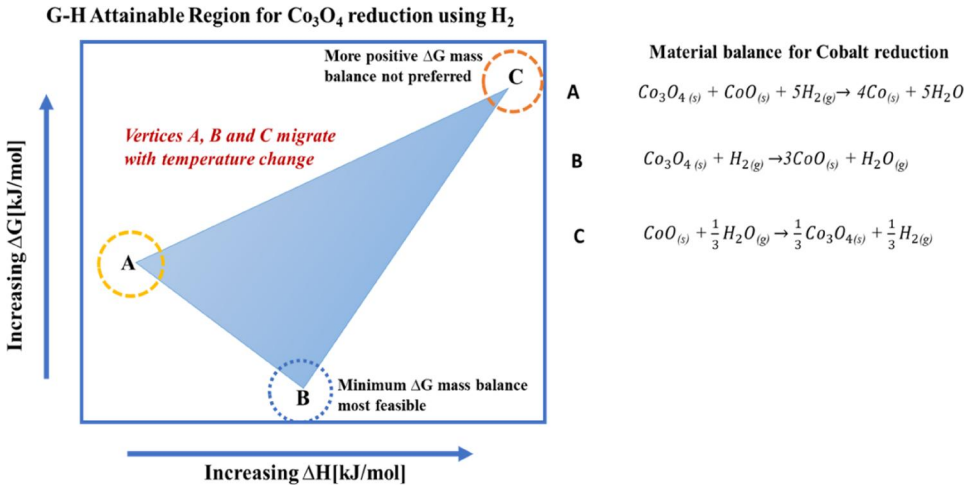



Figure 10. The prototypical G-H attainable region of the Co reduction system (vertices A, B and C) shows the G-H AR boundary vertices (Gorimbo et al. 2020).

Larger pores correspond to the formation of larger $Co_3O_4$ crystallite with decreased dispersion. Different pore sizes exhibited by supports result in varying CO adsorption properties. Supports with a pore size in the range of 6–10 nm have been shown to result in better FT activity and more selectivity to the desired $C_{5+}$. This observation is attributed to moderate crystallite size and CO adsorption on the catalyst (Song and Li 2006).

### Effect of promoters on crystallite size

In FT, promoters are chemical additives that enhance the physical, chemical and catalytic properties of the catalyst. In a study done by Jacobs et al. (2002) reduction temperature was significantly reduced by incorporating small amounts of Ru and Pt during the synthesis of a cobalt-based catalyst. Adding Mn has been shown to enhance metal cluster dispersion, which results in a smaller average size of cobalt crystallite (Sukkathanyawat et al. 2015). Mn also influences FTS product distribution by promoting the formation of long-chain hydrocarbon on a cobalt-supported catalyst (Sukkathanyawat et al. 2015). Morales et al. (2007) reported that MnO species cause positive structural and electronic modification of the catalyst, resulting in improved FT catalytic performance. Morales et al. (2007) also observed that the water gas shift (WGS) reaction was catalyzed by MnO, which adjusts the $H_2/CO$ ratio and alters overall FT catalytic performance. Alkali metals are also useful as FT catalyst chemical promoters, as they affect activity and selectivity. Performance evaluation of the $Co/Al_2O_3$ catalysts promoted Li, Na, K, Rb and Cs resulted in enhanced $C_{5+}$ selectivity (Gholami et al. 2021). Generally, the literature provides definitive evidence that promoters facilitate Co reducibility at a lower reduction temperature than non-promoted catalysts. Several detailed reviews and work on the effect of promoters are available (Shimura et al. 2015; Yang et al. 2022).

### *Concluding remarks*

The literature analysis indicates that the catalytic properties of small cobalt particles (<6nm) differ from those of larger ones (>6nm) in FT synthesis. Oxidation of cobalt particles less than 6 nm in diameter can be minimized by correctly adjusting the hydrogen and water partial pressure in the FT reactor. The crystallite diameter of cobalt particle size appears to be a parameter of influence in controlling speciation by oxidation of the cobalt catalyst. From the literature surveyed, the general conclusion is that cobalt crystallite size significantly affects product selectivity. Cobalt crystallite with a size of <6–8 nm tends to favor the formation of methane and reduce $C_{5+}$ selectivity. $C_{5+}$ products are the most sought-after product nowadays; hence its increased selectivity is ideal.

$H_2$ adsorption is the most convenient, accurate and generally applicable technique for estimating the average crystallite size of several FT catalysts. However, TEM is a precise technique for measuring the average crystallite size and the distribution of the size of the metal catalysts in FT. XRD is widely used in FT to determine crystallite size, although it is generally insensitive to small metal particles that are <3 nm. It is apparent that no single method fully characterizes crystallite size and distribution in supported metal catalysts in the absence of inherent theoretical shortcomings, uncertainty in the experimental approach and ambiguity in the interpretation of results. Therefore, it is ideal to use multiple techniques whenever possible to validate the readings obtained.

There are still challenges in precisely controlling the crystallite size at the nanoscale this demands advanced synthesis methods to ensure easy synthesis, uniformity and reproducibility. Another challenge is attributing FT activity to initial crystallite size. Therefore there is a need to capture and comprehend dynamic changes in crystallite size during different stages of FT reaction, this requires sophisticated in-situ characterization techniques. The interaction between cobalt crystallites and catalyst supports adds complexity. Optimizing this interplay to enhance stability and catalytic activity is an ongoing challenge.

Demonstrating the impact of particle or crystallite size at the laboratory scale is just the beginning. The translation of these findings to industrial-scale reactors presents additional

challenges due to limitations in heat and mass transfer, reactor design considerations, and potential catalyst deactivation effects. Therefore, it is crucial to understand the scalability of particle size effects for practical implementation.

***Perspectives:***

1. Debunking the impact of particle and crystallite size in cobalt-based Fisher-Tropsch synthesis presents a crucial opportunity to deepen our fundamental understanding of the underlying mechanisms governing catalytic reactions. This understanding can greatly aid in designing more efficient and selective catalysts for industrial applications. By acquiring knowledge of the underlying processes that govern catalytic reactions, it becomes possible to optimize and improve the performance of catalysts for specific applications. Therefore, this study represents an important step toward the development of more effective and efficient catalytic processes, which can help to drive industrial innovation and progress.
2. The study of particle and crystallite size impact on catalyst optimization is crucial for identifying the optimal catalyst sizes that maximize desired product selectivity or improve activity. This knowledge is invaluable in the development of more efficient and cost-effective cobalt-based Fischer-Tropsch catalysts. By utilizing the insights gained from this study, it is possible to guide the development of optimized catalysts that will lead to higher product yields, lower costs, and increased sustainability.
3. Process intensification is a crucial aspect of chemical engineering, and understanding the role of particle/crystallite size can significantly aid in developing strategies for process intensification. By designing catalysts with tailored properties, it may be possible to achieve higher conversion and selectivity within smaller reactor volumes, especially if smaller particles exhibit higher activity. Therefore, particle/crystallite size should be a key consideration in the design of catalysts and reactors to achieve optimal process intensification.
4. The stability of a catalyst plays a crucial role in industrial and academic settings. The impact of particle/crystallite size on catalyst stability is a subject of significant research, as it provides valuable insights into potential deactivation mechanisms. Investigating this impact enables the identification of ways to enhance catalyst longevity by mitigating particle sintering, maintaining active site accessibility, or improving resistance to catalyst poisons. These insights can help design more robust catalysts and contribute to the development of efficient and sustainable chemical processes.
5. Catalyst design and engineering: Insights gained from studying particle/crystallite size effects can contribute to more rational catalyst design and engineering. Optimizing particle sizes, surface structures, and interactions can lead to enhanced catalytic performance and overall process efficiency.
6. Finally, the integration of cutting-edge techniques such as in-situ microscopy and spectroscopy offers a promising perspective for unraveling real-time changes in crystallite size during Fischer-Tropsch reactions.

The perspectives presented in this study highlight the potential for gaining fundamental knowledge, optimizing catalysts, improving process intensification, enhancing catalyst stability, and enabling rational catalyst design and engineering. Therefore, it is essential to consider these perspectives when exploring cobalt-based Fisher-Tropsch synthesis and its potential applications.

## Acknowledgements

The author would like to acknowledge the University of South Africa (UNISA), Institute of Development of Energy for African Sustainability (IDEAs), and National Research Fund (NRF) for funding.

## Disclosure statement

The authors declare no conflict of interest.

## References


Alexander L, Klug HP. 1950. Determination of crystallite size with the x-ray spectrometer. J Appl Phys. 21(2):137–142. doi:10.1063/1.1699612.

Almithn AS, Hibbitts DD. 2018. Supra-monolayer coverages on small metal clusters and their effects on $H_2$ chemisorption particle size estimates. AIChE J. 64(8):3109–3120. doi:10.1002/aic.16110.

Bao A, Liew K, Li J. 2009. Fischer–Tropsch synthesis on CaO-promoted $Co/Al_2O_3$ catalysts. J Mol Catal. Chem. 304(1–2):47–51. doi:10.1016/j.molcata.2009.01.022.

Bezemer GL, Bitter JH, Kuipers HP, Oosterbeek H, Holewijn JE, Xu X, Kapteijn F, Van Dillen AJ, de Jong KP. 2006. Cobalt particle size effects in the Fischer – Tropsch reaction studied with carbon nanofiber supported catalysts. J Am Chem Soc. 128(12):3956–3964. doi:10.1021/ja058282w.

Bian G-Z, Fujishita N, Mochizuki T, Ning W-S, Yamada M. 2003. Investigations on the structural changes of two $Co/SiO_2$ catalysts by performing Fischer–Tropsch synthesis. Appl Catal Gen. 252(2):251–260. doi:10.1016/S0926-860X(03)00470-8.

Bianchi CL, Martini F, Moggi P. 2001. $Co/SiO_2$ sol–gel catalysts for Fischer–Tropsch synthesis. Catal Lett. 76(1/2):65–69. doi:10.1023/A:1016712507527.

Borg Ø, Dietzel PD, Spjelkavik AI, Tveten EZ, Walmsley JC, Diplas S, Eri S, Holmen A, Rytter E. 2008. Fischer–Tropsch synthesis: cobalt particle size and support effects on intrinsic activity and product distribution. J Catal. 259(2):161–164. doi:10.1016/j.jcat.2008.08.017.

Borg O, Eri S, Blekkan E, Storsater S, Wigum H, Rytter E, Holmen A. 2007. Fischer–Tropsch synthesis over $\gamma$-alumina-supported cobalt catalysts: effect of support variables. J Catal. 248(1):89–100., doi:10.1016/j.jcat.2007.03.008.

Bosch H, Kip BJ, Van Ommen JG, Gellings PJ. 1984. Factors influencing the temperature-programmed reduction profiles of vanadium pentoxide. J Chem Soc, Faraday Trans 1. 80(9):2479–2488. doi:10.1039/f19848002479.

Brunner KM, Huang B, Woodfield BF, Hecker WC. 2015a. Iron fischer-tropsch catalysts prepared by solvent-deficient precipitation (SDP): effects of washing, promoter addition step, and drying temperature. Catalysts. 5(3):1352–1374. doi:10.3390/catal5031352.

Brunner KM, Perez HD, Peguin RP, Duncan JC, Harrison LD, Bartholomew CH, Hecker WC. 2015b. Effects of particle size and shape on the performance of a trickle fixed-bed recycle reactor for Fischer–Tropsch synthesis. Ind Eng Chem Res. 54(11):2902–2909. doi:10.1021/ie503174v.

Bushroa AR, Rahbari RG, Masjuki HH, Muhamad MR. 2012. Approximation of crystallite size and microstrain via XRD line broadening analysis in TiSiN thin films. Vacuum. 86(8):1107–1112. doi:10.1016/j.vacuum.2011.10.011.

Bykova M, Ermakov DY, Kaichev V, Bulavchenko O, Saraev A, Lebedev MY, Yakovlev V. 2012. Ni-based sol–gel catalysts as promising systems for crude bio-oil upgrading: guaiacol hydrodeoxygenation study. Appl Catal B Environ. 113-114:296–307. doi:10.1016/j.apcatb.2011.11.051.

Chauhan A, Chauhan P. 2014. Powder XRD technique and its applications in science and technology. J Anal Bioanal Tech. 5(6):1–5. doi:10.4172/2155-9872.1000212.

Cheng Q, Tian Y, Lyu S, Zhao N, Ma K, Ding T, Jiang Z, Wang L, Zhang J, Zheng L, et al. 2018. Confined small-sized cobalt catalysts stimulate carbon-chain growth reversely by modifying ASF law of Fischer–Tropsch synthesis. Nat Commun. 9(1):3250., doi:10.1038/s41467-018-05755-8.

Choudhury H, Cheng X, Afzal S, Prakash A, Tatarchuk B, Elbashir N. 2020. Understanding the deactivation process of a microfibrous entrapped cobalt catalyst in supercritical fluid Fischer-Tropsch synthesis. Catal Today. 343:112–124. doi:10.1016/j.cattod.2019.01.031.

Christel L, Pierre A, Abel DA-MR. 1997. Temperature programmed reduction studies of nickel manganite spinels. Thermochim Acta. 306(1-2):51–59. doi:10.1016/S0040-6031(97)00299-2.

Den Breejen JP, Radstake PB, Bezemer GL, Bitter JH, Frøseth V, Holmen A, De Jong KP. 2009. On the origin of the cobalt particle size effects in Fischer-Tropsch catalysis. J Am Chem Soc. 131(20):7197–7203. doi:10.1021/ja901006x.

Deraz N. 2018. The comparative jurisprudence of catalysts preparation methods: I. Precipitation and Impregnation Methods. J Ind Env Chem. 2:19–21.

Deugd RMD, Ypma SM, Kapteijn F, Meeuse FM, Moulijn JA, Verheijen PJT. 2001. Model-based optimization of the periodic operation of the Fischer-Tropsch synthesis**This work is part of Delft Interdisciplinary Research Centre "Mastering the Molecules in Manufacturing. In: Froment, GF, Waugh, KC, editor. Reaction kinetics and the development and operation of catalytic processes, studies in surface science and catalysis, p. 255–262. doi:10.1016/S0167-2991(01)81970-4.

Fang X, Liu B, Cao K, Yang P, Zhao Q, Jiang F, Xu Y, Chen R, Liu X. 2020. Particle-size-dependent methane selectivity evolution in Cobalt-based Fischer–Tropsch synthesis. ACS Catal. 10(4):2799–2816. doi:10.1021/acscatal.9b05371.

Fierro G, Lojacono M, Inversi M, Porta P, Lavecchia R, Cioci F. 1994. A study of anomalous temperature-programmed reduction profiles of $Cu_2O$, CuO, and CuO-ZnO catalysts. J Catal. 148(2):709–721. doi:10.1006/jcat.1994.1257.

Fischer N, Clapham B, Feltes T, van Steen E, Claeys M. 2014. Size-dependent phase transformation of catalytically active nanoparticles captured in situ. Angew Chem. 126(5):1366–1369. doi:10.1002/ange.201306899.

Fischer N, Van Steen E, Claeys M. 2013. Structure sensitivity of the Fischer-Tropsch activity and selectivity on alumina supported cobalt catalysts. J Catal. 299:67–80. doi:10.1016/j.jcat.2012.11.013.

Fisker R, Carstensen JM, Hansen MF, Bødker F, Mørup S. 2000. Estimation of nanoparticle size distributions by

image analysis. J Nanoparticle Res. 2(3):267–277. doi:10.1023/A:1010023316775.

Fu T, Lv J, Li Z. 2014. Effect of carbon porosity and cobalt particle size on the catalytic performance of carbon supported cobalt fischer-tropsch catalysts. Ind Eng Chem Res. 53(4):1342–1350. doi:10.1021/ie402128y.

García-Sánchez JT, Baldovino-Medrano VG. 2023. Elements of the Manufacture and Properties of Technical Catalysts. Ind Eng Chem Res. 62(20):7769–7838. doi:10.1021/acs.iecr.3c00369.

Gavrilović L, Brandin J, Holmen A, Venvik HJ, Myrstad R, Blekkan EA. 2018. Fischer-Tropsch synthesis—Investigation of the deactivation of a Co catalyst by exposure to aerosol particles of potassium salt. Appl Catal B Environ. 230:203–209. doi:10.1016/j.apcatb.2018.02.048.

Geyer R, Hunold J, Keck M, Kraak P, Pachulski A, Schödel R. 2012. Methods for determining the metal crystallite size of Ni supported catalysts. Chem Ing Tech. 84(1-2):160–164. doi:10.1002/cite.201100101.

Ghogia AC, Nzihou A, Serp P, Soulantica K, Pham Minh D. 2021. Cobalt catalysts on carbon-based materials for Fischer-Tropsch synthesis: a review. Appl Catal Gen. 609:117906. doi:10.1016/j.apcata.2020.117906.

Gholami Z, Tišler Z, Rubáš V. 2021. Recent advances in Fischer-Tropsch synthesis using cobalt-based catalysts: a review on supports, promoters, and reactors. Catal Rev Sci Eng. 63(3):512–595. doi:10.1080/01614940.2020.1762367.

Giordano F, Trovarelli A, de Leitenburg C, Giona M. 2000. A model for the temperature-programmed reduction of low and high surface area ceria. J Catal. 193(2):273–282. doi:10.1006/jcat.2000.2900.

Gontard LC, Ozkaya D, Dunin-Borkowski RE. 2011. A simple algorithm for measuring particle size distributions on an uneven background from TEM images. Ultramicroscopy. 111(2):101–106. doi:10.1016/j.ultramic.2010.10.011.

Gorimbo J. 2016. An experimental and thermodynamic study of iron catalyst activation and deactivation during Fischer Tropsch synthesis. University of the Witwatersrand.

Gorimbo J. 2018. Use of stability diagrams to predict catalyst speciation during Fischer Tropsch reduction stage: a mini-review. Catal Sci Technol. 8(8):2022–2029. doi:10.1039/C8CY00228B.

Gorimbo J, Muvhiiwa R, Llane E, Hildebrandt D. 2020. Cobalt catalyst reduction thermodynamics in Fischer Tropsch: an attainable region approach. Reactions. 1(2):115–129. doi:10.3390/reactions1020010.

Green H. 1927. The effect of non-uniformity and particulate shape on "average particle' size. J Frankl. Inst. 204(6):713–729. doi:10.1016/S0016-0032(27)92037-7.

Haber J. 1991. Manual on catalyst characterization. Pure Appl Chem. 63(9):1227–1246. doi:10.1351/pac199163091227.

Hatch T. 1933. Determination of "average particle size" from the screen-analysis of non-uniform particulate substances. J Frankl Inst. 215(1):27–37. doi:10.1016/S0016-0032(33)90137-4.

Herranz T, Deng X, Cabot A, Guo J, Salmeron M. 2009. Influence of the cobalt particle size in the CO hydrogenation reaction studied by in situ X-ray absorption spectroscopy. J Phys Chem B. 113(31):10721–10727. doi:10.1021/jp901602s.

Heywood H. 2010. Numerical definitions of particle size and shape. J Chem Technol Biotechnol. 56(7):149–154. doi:10.1002/jctb.5000560702.

Hilmen A, Schanke D, Hanssen K, Holmen A. 1999. Study of the effect of water on alumina supported cobalt Fischer–Tropsch catalysts. Appl Catal Gen. 186(1-2):169–188. doi:10.1016/S0926-860X(99)00171-4.

Hu J, Yu F, Lu Y. 2012. Application of Fischer–Tropsch synthesis in biomass to liquid conversion. Catalysts. 2(2):303–326. doi:10.3390/catal2020303.

Iglesia E. 1997a. Fischer-Tropsch synthesis on cobalt catalysts: structural requirements and reaction pathways. Stud Surf Sci Catal. 107:153–162.

Iglesia E. 1997b. Design, synthesis, and use of cobalt-based Fischer-Tropsch synthesis catalysts. Appl Catal Gen. 161(1-2):59–78. doi:10.1016/S0926-860X(97)00186-5.

Jacobs G, Das TK, Patterson PM, Li J, Sanchez L, Davis BH. 2003. Fischer–Tropsch synthesis XAFS: XAFS studies of the effect of water on a Pt-promoted $Co/Al_2O_3$ catalyst. Appl Catal Gen. 247(2):335–343. doi:10.1016/S0926-860X(03)00107-8.

Jacobs G, Das TK, Zhang Y, Li J, Racoillet G, Davis BH. 2002. Fischer-Tropsch synthesis: support, loading, and promoter effects on the reducibility of cobalt catalysts. Appl Catal Gen. 233(1–2):263–281. doi:10.1016/S0926-860X(02)00195-3.

Jacobs G, Ji Y, Davis BH, Cronauer D, Kropf AJ, Marshall CL. 2007. Fischer–Tropsch synthesis: temperature programmed EXAFS/XANES investigation of the influence of support type, cobalt loading, and noble metal promoter addition to the reduction behavior of cobalt oxide particles. Appl Catal Gen. 333(2):177–191. doi:10.1016/j.apcata.2007.07.027.

James OO, Maity S. 2016. Temperature programme reduction (TPR) studies of cobalt phases in-alumina supported cobalt catalysts. J Pet Technol Altern Fuels. 7:1–12.

Jozwiak W, Kaczmarek E, Maniecki T, Ignaczak W, Maniukiewicz W. 2007. Reduction behavior of iron oxides in hydrogen and carbon monoxide atmospheres. Appl Catal Gen. 326(1):17–27. doi:10.1016/j.apcata.2007.03.021.

Kazemnejad I, Feizbakhsh A, Niazi A, Tavasoli A. 2019. Highly dispersed cobalt Fischer–Tropsch synthesis catalysts supported on $\gamma$-$Al_2O_3$, CNTs, and graphene nanosheet using chemical vapor deposition. Int J Ind Chem. 10(4):321–333. doi:10.1007/s40090-019-00195-9.

Kliewer C, Soled S, Kiss G. 2019. Morphological transformations during Fischer-Tropsch synthesis on a titania-supported cobalt catalyst. Catal Today. 323:233–256. doi:10.1016/j.cattod.2018.05.021.

Langford JL, Wilson JC. 1978. Scherrer after sixty years: a survey and some new results in the determination of

crystallite size. J Appl Crystallogr. 11(2):102–113. doi:10.1061/9780784479896.140.

Lele S, Anantharaman TR. 1962. Influence of crystallite shape on particle size broadening of Debye-Scherrer reflections, in. Proc Indian Acad Sci. 64(5):261–274. doi:10.1007/BF03047543.

Li J, Jacobs G, Das T, Zhang Y, Davis B. 2002. Fischer–Tropsch synthesis: effect of water on the catalytic properties of a Co/$SiO_2$ catalyst. Appl Catal Gen. 236(1-2):67–76. doi:10.1016/S0926-860X(02)00276-4.

Li Q, Kartikowati CW, Horie S, Ogi T, Iwaki T, Okuyama K. 2017. Correlation between particle size/domain structure and magnetic properties of highly crystalline $Fe_3O_4$ nanoparticles. Sci Rep. 7(1):9894. doi:10.1038/s41598-017-09897-5.

Lira E, López CM, Oropeza F, Bartolini M, Alvarez J, Goldwasser M, Linares FL, Lamonier J-F, Zurita, MJP. 2008. HMS mesoporous silica as cobalt support for the Fischer–Tropsch Synthesis: pretreatment, cobalt loading and particle size effects. J Mol Catal Chem. 281(1-2):146–153. doi:10.1016/j.molcata.2007.11.014.

Liu Y, Fang K, Chen J, Sun Y. 2007. Effect of pore size on the performance of mesoporous zirconia-supported cobalt Fischer–Tropsch catalysts. Green Chem. 9(6):611–615. doi:10.1039/B614266D.

Liu K, Suo H, Zhang C, Xu J, Yang Y, Xiang H, Li Y. 2010. An active Fischer–Tropsch synthesis FeMo/$SiO_2$ catalyst prepared by a modified sol–gel technique. Catal Commun. 12(2):137–141. doi:10.1016/j.catcom.2010.09.007.

Li H, Wang S, Ling F, Li J. 2006. Studies on MCM-48 supported cobalt catalyst for Fischer-Tropsch synthesis. J Mol Catal Chem. 244(1-2):33–40. doi:10.1016/j.molcata.2005.08.050.

Louër D, Weigel D, Langford JI. 1972. Etude des profils de raies de diffraction des rayons X d'une poudre d'hydroxyde de nickel. J Appl Crystallogr. 5(5):353–359. doi:10.1107/S0021889872009756.

Lu X. 2011. Fischer-Tropsch synthesis: towards understanding. Univ. Witwatersrand.

Ma W, Dalai AK. 2021. Effects of structure and particle size of iron, cobalt and ruthenium catalysts on Fischer–Tropsch Synthesis. Reactions. 2(1):62–77. doi:10.3390/reactions2010006.

Malet P, Caballero A. 1988. The selection of experimental conditions in temperature-programmed reduction experiments. J Chem Soc Faraday Trans 1. 84(7):2369–2375. doi:10.1039/f19888402369.

Martínez A, López C, Márquez F, Díaz I. 2003. Fischer–Tropsch synthesis of hydrocarbons over mesoporous Co/SBA-15 catalysts: the influence of metal loading, cobalt precursor, and promoters. J Catal. 220(2):486–499. doi:10.1016/S0021-9517(03)00289-6.

Matyi R, Schwartz L, Butt J. 1987. Particle size, particle size distribution, and related measurements of supported metal catalysts. Catal Rev Sci Eng. 29(1):41–99. doi:10.1080/01614948708067547.

Matyi RJ, Schwartz LH, Butt JB. 1987. Particle size, particle size distribution, and related measurements of supported metal catalysts. Catal Rev. 29(1):41–99. doi:10.1080/01614948708067547.

Melaet G, Lindeman AE, Somorjai GA. 2014. Cobalt particle size effects in the Fischer-Tropsch synthesis and in the hydrogenation of $CO_2$ studied with nanoparticle model catalysts on silica. Top Catal. 57(6-9):500–507. doi:10.1007/s11244-013-0206-z.

Miller J, Meyers B, Modica F, Lane G, Vaarkamp M, Koningsberger D. 1993. Hydrogen temperature-programmed desorption ($H_2$ TPD) of supported platinum catalysts. J Catal. 143(2):395–408. doi:10.1006/jcat.1993.1285.

Mitchell S, Michels N-L, Pérez-Ramírez J. 2013. From powder to technical body: the undervalued science of catalyst scale up. Chem Soc Rev. 42(14):6094–6112. doi:10.1039/c3cs60076a.

Modekwe HU, Mamo MA, Moothi K, Daramola MO. 2021. Effect of different catalyst supports on the quality, yield and morphology of carbon nanotubes produced from waste polypropylene plastics. Catalysts. 11(6):692. doi:10.3390/catal11060692.

Monshi A, Foroughi MR, Monshi MR. 2012. Modified Scherrer equation to estimate more accurately nano-crystallite size using XRD. WJNSE. 02(03):154–160. doi:10.4236/wjnse.2012.23020.

Morales F, de Smit E, de Groot FMF, Visser T, Weckhuysen BM. 2007. Effects of manganese oxide promoter on the CO and $H_2$ adsorption properties of titania-supported cobalt Fischer-Tropsch catalysts. J Catal. 246(1):91–99. doi:10.1016/j.jcat.2006.11.014.

Muniz FTL, Miranda MAR, Morilla Dos Santos C, Sasaki JM. 2016. The Scherrer equation and the dynamical theory of X-ray diffraction. Acta Crystallogr A Found Adv. 72(Pt 3):385–390. doi:10.1107/S205327331600365X.

Mustard DG, Bartholomew CH. 1981. Determination of metal crystallite size and morphology in supported nickel catalysts. J Catal. 67(1):186–206. doi:10.1016/0021-9517(81)90271-2.

Okabe K, Li X, Wei M, Arakawa H. 2004. Fischer–Tropsch synthesis over Co–SiO2 catalysts prepared by the sol–gel method. Catal Today. 89(4):431–438. doi:10.1016/j.cattod.2004.01.005.

Okoye-Chine CG, Forbes R, Gorimbo J, Moyo M, Liu X, Hildebrandt D. 2023. The effect of pretreatment on $SiO_2$ for Co-based Fischer-Tropsch synthesis catalysts: a study of the reduction pathway. Chem Eng Commun. 210(7):1097–1107. doi:10.1080/00986445.2022.2056452.

Parker SF, Walker HC, Callear SK, Grünewald E, Petzold T, Wolf D, Möbus K, Adam J, Wieland SD, Jiménez-Ruiz M, et al. 2019. The effect of particle size, morphology and support on the formation of palladium hydride in commercial catalysts. Chem Sci. 10(2):480–489., doi:10.1039/c8sc03766c.

Petersen AP, Claeys M, Kooyman PJ, van Steen E. 2019. Cobalt-based Fischer–Tropsch synthesis: a kinetic

evaluation of metal–support interactions using an inverse model system. Catalysts. 9(10):794. doi:10.3390/catal9100794.

Pratt JW. …. 2012. A Fischer-Tropsch synthesis reactor model framework for liquid biofuels production. Albuquerque, NM, and Livermore, CA: Sandia National Laboratories (SNL).

Prieto G, Martínez A, Concepción P, Moreno-Tost R. 2009. Cobalt particle size effects in Fischer–Tropsch synthesis: structural and in situ spectroscopic characterisation on reverse micelle-synthesised Co/ITQ-2 model catalysts. J Catal. 266(1):129–144. doi:10.1016/j.jcat.2009.06.001.

Pyrz WD, Buttrey DJ. 2008. Particle size determination using TEM: a discussion of image acquisition and analysis for the novice microscopist. Langmuir. 24(20): 11350–11360. doi:10.1021/la801367j.

Rane S, Borg Ø, Rytter E, Holmen A. 2012. Relation between hydrocarbon selectivity and cobalt particle size for alumina supported cobalt Fischer–Tropsch catalysts. Appl Catal Gen. 437-438:10–17. doi:10.1016/j.apcata.2012.06.005.

Ratchananusorn W. 2007. Flow phenomena, heat and mass transfer in microchannel reactors.

Rozita Y, Brydson R, Scott A. 2010. An investigation of commercial gamma-Al2O3 nanoparticles. J Phys Conf Ser. 241IOP Publishing, :012096. doi:10.1088/1742-6596/241/1/012096.

Rytter E, Borg Ø, Tsakoumis NE, Holmen A. 2018. Water as key to activity and selectivity in Co Fischer-Tropsch synthesis: γ-alumina based structure-performance relationships. J Catal. 365:334–343. doi:10.1016/j.jcat.2018.07.003.

Rytter E, Holmen A. 2015. Deactivation and regeneration of commercial type Fischer-Tropsch Co-catalysts—A mini-review. Catalysts. 5(2):478–499. doi:10.3390/catal5020478.

Saib A, Claeys M, Van Steen E. 2002. Silica supported cobalt Fischer–Tropsch catalysts: effect of pore diameter of support. Catal Today. 71(3-4):395–402. doi:10.1016/S0920-5861(01)00466-7.

Saib A, Moodley D, Ciobîcă I, Hauman M, Sigwebela B, Weststrate C, Niemantsverdriet J, Van de Loosdrecht J. 2010. Fundamental understanding of deactivation and regeneration of cobalt Fischer–Tropsch synthesis catalysts. Catal Today. 154(3-4):271–282. doi:10.1016/j.cattod.2010.02.008.

Satterfield CN, Pelossof AA, Sherwood TK. 1969. Mass transfer limitations in a trickle-bed reactor. AlChE J. 15(2):226–234. doi:10.1002/aic.690150219.

Schanke D, Hilmen AM, Bergene E, Kinnari K, Rytter E, Dnanes E, Holmen A. 1995. Study of the deactivation mechanism of $Al_2O_3$-supported cobalt Fischer-Tropsch catalysts. Catal Lett. 34(3-4):269–284., doi:10.1007/BF00806876.

Shimura K, Miyazawa T, Hanaoka T, Hirata S. 2015. Fischer–Tropsch synthesis over alumina supported cobalt catalyst: Effect of promoter addition. Appl Catal Gen. 494:1–11. doi:10.1016/j.apcata.2015.01.017.

Smith JM, Ness HCV, Abbott MM, Swihart MT. 2018. Introduction to chemical engineering thermodynamics. New York: McGraw Hill Education doi:10.1021/ed027p584.3.

Song D, Li J. 2006. Effect of catalyst pore size on the catalytic performance of silica supported cobalt Fischer-Tropsch catalysts. J Mol Catal Chem. 247(1-2):206–212. doi:10.1016/j.molcata.2005.11.021.

Soykal II, Sohn H, Ozkan US. 2012. Effect of support particle size in steam reforming of ethanol over $Co/CeO_2$ catalysts. ACS Catal. 2(11):2335–2348. doi:10.1021/cs3004159.

Stamenić M, Dikić V, Mandić M, Todić B, Bukur DB, Nikačević NM. 2018. Multiscale and multiphase model of fixed-bed reactors for Fischer–Tropsch Synthesis: optimization Study. Ind Eng Chem Res. 57(9):3149–3162. doi:10.1021/acs.iecr.7b04914.

Sukkathanyawat H, Tungkamani S, Phongaksorn M, Rattana T, Narataruksa P, Yoosuk B. 2015. Promoter effect on the physico-chemical properties of cobalt based catalyst for CO hydrogenation. Energy Procedia. 79:372–377. doi:10.1016/j.egypro.2015.11.505.

Thiele EW. 1939. Relation between Catalytic Activity and Size of Particle. Ind Eng Chem. 31(7):916–920. doi:10.1021/ie50355a027.

Tsubaki N, Zhang Y, Sun S, Mori H, Yoneyama Y, Li X, Fujimoto K. 2001. A new method of bimodal support preparation and its application in Fischer–Tropsch synthesis. Catal Commun. 2(10):311–315. doi:10.1016/S1566-7367(01)00055-3.

Van Berge P, Van de Loosdrecht J, Barradas S, Van Der Kraan A. 2000. Oxidation of cobalt based Fischer–Tropsch catalysts as a deactivation mechanism. Catal Today. 58(4): 321–334. doi:10.1016/S0920-5861(00)00265-0.

van Steen E, Claeys M, Dry ME, van de Loosdrecht J, Viljoen EL, Visagie JL. 2005. Stability of nanocrystals: thermodynamic analysis of oxidation and re-reduction of cobalt in water/hydrogen mixtures. J Phys Chem B. 109(8):3575–3577. doi:10.1021/jp045136o.

Vorokh AS. 2018. Scherrer formula: estimation of error in determining small nanoparticle size. Nanosystems Phys Chem Math. 9:364–369. doi:10.17586/2220-8054-2018-9-3-364-369.

Wang H, Lu J. 2020. A review on particle size effect in metal-catalyzed heterogeneous reactions. Chin J Chem. 38(11):1422–1444. doi:10.1002/cjoc.202000205.

Wang Z, Skiles S, Yang F, Yan Z, Goodman DW. 2012. Particle size effects in Fischer–Tropsch synthesis by cobalt. Catal Today. 181(1):75–81. doi:10.1016/j.cattod.2011.06.021.

Wang H, Wang Z, Wang S, Yang C, Li S, Gao P, Sun Y. 2021. The effect of the particle size on Fischer–Tropsch synthesis for ZSM-5 zeolite supported cobalt-based catalysts. Chem Commun (Camb). 57(99):13522–13525. doi:10.1039/d1cc04844a.

Webb PA. 2003. Introduction to chemical adsorption analytical techniques and their applications to catalysis. Micromeritics Instrum Corp Tech Publ. 1–12.

Wilson AJC. 1969. Variance Apparent Particle Sizes for Cylinders, Prisms and Hemispheres. J Appl Crystallogr. 2(4):181–183. doi:10.1107/S0021889869006893.

Witoon T, Chareonpanich M, Limtrakul J. 2011. Effect of hierarchical meso-macroporous silica supports on Fischer-Tropsch synthesis using cobalt catalyst. Fuel Process Technol. 92(8):1498–1505. doi:10.1016/j.fuproc.2011.03.011.

Wolf M, Fischer N, Claeys M. 2021. Formation of metal-support compounds in cobalt-based Fischer-Tropsch synthesis: a review. Chem Catal. 1(5):1014–1041. doi:10.1016/j.checat.2021.08.002.

Xie W, Zhang Y, Liew K, Li J. 2012. Effect of catalyst confinement and pore size on Fischer-Tropsch synthesis over cobalt supported on carbon nanotubes. Sci China Chem. 55(9):1811–1818. doi:10.1007/s11426-012-4727-2.

Xiong H, Zhang Y, Wang S, Li J. 2005. Fischer–Tropsch synthesis: the effect of Al2O3 porosity on the performance of $Co/Al_2O_3$ catalyst. Catal Commun. 6(8):512–516. doi:10.1016/j.catcom.2005.04.018.

Yan P, Kennedy E, Stockenhuber M. 2021. Natural zeolite supported Ni catalysts for hydrodeoxygenation of anisole. Green Chem. 23(13):4673–4684. doi:10.1039/D0GC04377J.

Yang J, Frøseth V, Chen D, Holmen A. 2016. Particle size effect for cobalt Fischer–Tropsch catalysts based on in situ CO chemisorption. Surf Sci. 648:67–73. doi:10.1016/j.susc.2015.10.029.

Yang JH, Kim H-J, Chun DH, Lee H-T, Hong J-C, Jung H, Yang J-I. 2010. Mass transfer limitations on fixed-bed reactor for Fischer–Tropsch synthesis. Fuel Process. Technol. 91(3):285–289. doi:10.1016/j.fuproc.2009.10.010.

Yang X, Yang J, Zhao T, Qian W, Wang Y, Holmen A, Jiang W, Chen D, Ben H. 2022. Kinetic insights into the effect of promoters on $Co/Al_2O_3$ for Fischer-Tropsch synthesis. Chem Eng J. 445:136655. doi:10.1016/j.cej.2022.136655.

Zeng B, Hou B, Jia L, Wang J, Chen C, Sun Y, Li D. 2013. Studies of cobalt particle size effects on Fischer–Tropsch synthesis over core–shell-structured catalysts. Chem Cat Chem. 5(12):3794–3801. doi:10.1002/cctc.201300471.

Zhai P, Sun G, Zhu Q, Ma D. 2013. Fischer-Tropsch synthesis nanostructured catalysts: understanding structural characteristics and catalytic reaction. Nanotechnol Rev. 2(5):547–576. doi:10.1515/ntrev-2013-0025.

Zhang Y, Hanayama K, Tsubaki N. 2006. The surface modification effects of silica support by organic solvents for Fischer-Tropsch synthesis catalysts. Catal Commun. 7(5):251–254. doi:10.1016/j.catcom.2005.11.008.

Zhou X, Xu W, Liu G, Panda D, Chen P. 2010. Size-dependent catalytic activity and dynamics of gold nanoparticles at the single-molecule level. J Am Chem Soc. 132(1):138–146. doi:10.1021/ja904307n.